CHAPTER IV

TELEMETRY DESIGN

By Walt C. Long
Langley Research Center

SECTION I - INTRODUCTION

The basic telemetry-system concept for Explorer XIII was selected primarily on the basis of demonstrated performance (ref. IV-1). The successful orbiting of Vanguard II (1959 Alpha) and Vanguard III (1959 Eta) had proven the basic design of the tracking and telemetry concepts which were compatible with minitrack network. It was necessary for the NASA Langley Research Center (LRC) to expand the system to provide a 48-channel telemetry system. Two of these systems were used in the Explorer XIII in order to provide the required channel capacity.

A study of the anticipated data revealed that the prime data (the micrometeoroid-penetration data) would occur at an extremely slow rate and that one data readout per day from the satellite would be adequate to satisfy the needs of the program. Some of the secondary data would have been made more meaningful by obtaining real-time data, but it was believed that the results would not justify the complexity and effort that would have been required. A study revealed that the penetration detectors gave a permanent and irreversible output upon being penetrated by a micrometeoroid and that the impact detectors gave a momentary pulse output upon micrometeoric collision. Therefore, data storage was inherent in the penetration detectors but was required for the impact detectors. An events-counting and storing system was provided with sufficient capacity to allow up to 24 hours to elapse between readouts with little chance of recycling between readouts.

In the planned orbit, transmission ranges would be not less than 244 nautical miles (perigee) under any condition and quite often would be as great as 1,000 nautical miles. The radio-frequency links were therefore designed for the 1,000-nautical-mile range. The calculated signal-to-noise ratios are shown in figure IV-1. From this figure, it can be seen that little difficulty was anticipated in the data acquisition and data reduction. Section IV of this chapter and Section IV of Chapter VIII give some of the operational results.

SECTION II - SYSTEMS DESCRIPTION

The telemetry system for Explorer XIII consisted of two separate and independent telemeters for data transmission and a radio beacon for tracking. The two telemeters were of the data storage-command readout type wherein data were collected during the satellite's orbit(s) and read out when within range of a ground receiving station. Data storage was sufficient to allow up to 24 hours

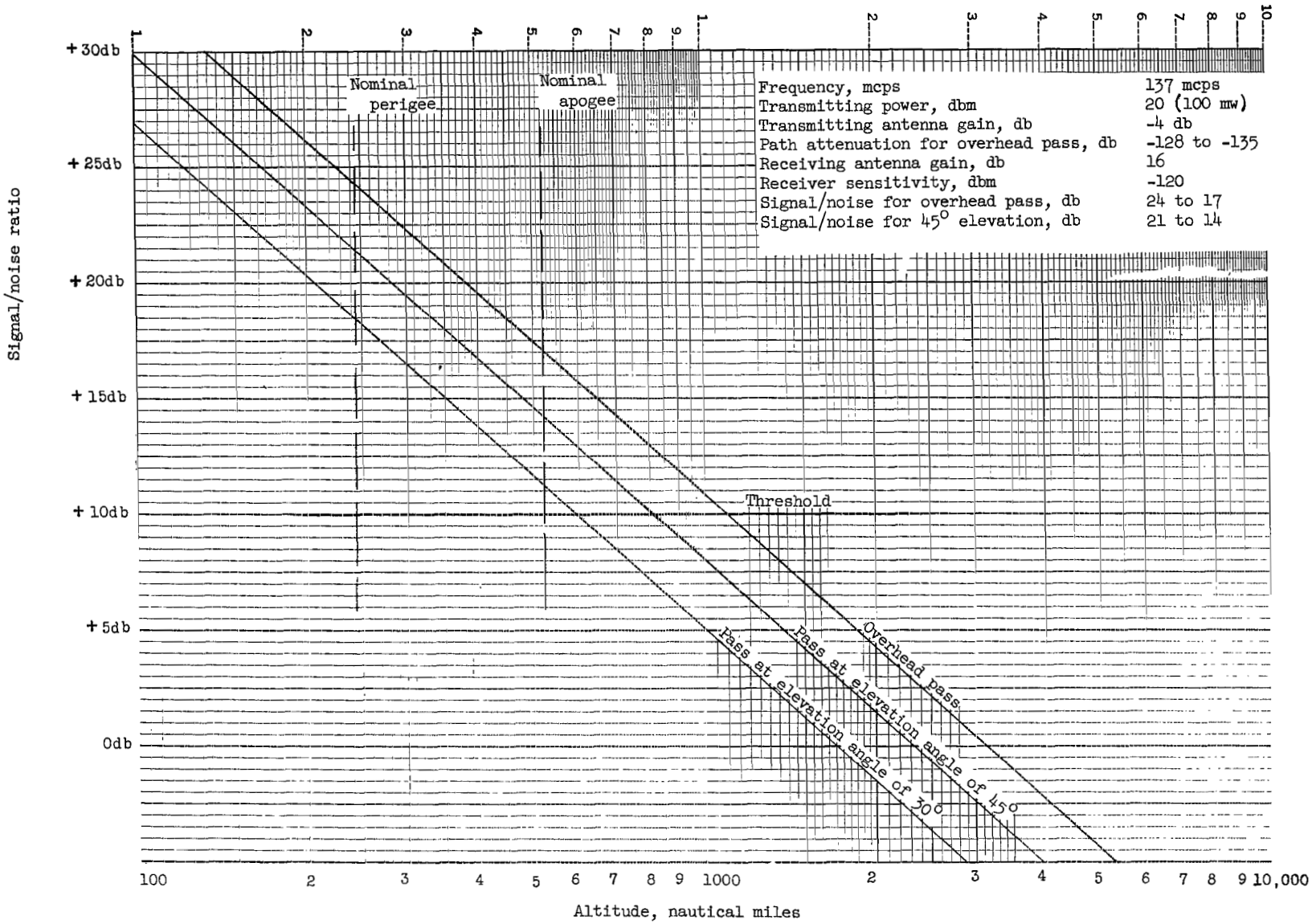

Figure IV-1.- Anticipated signal-to-noise ratios.

to elapse between readouts. Readout was nondestructive in that stored data were not erased. Two radio frequencies were used for data transmission, but only one command radio frequency was used for interrogation.

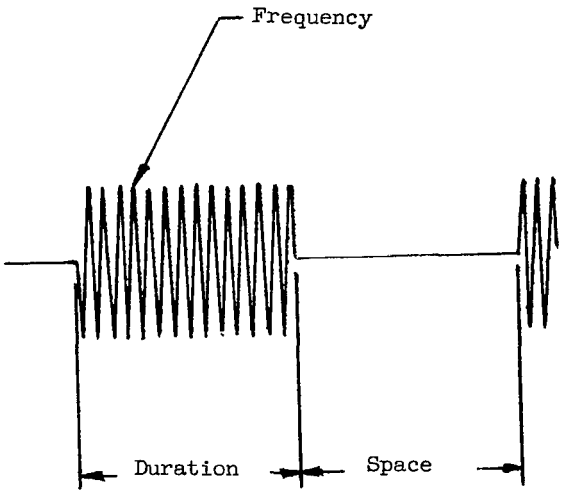

Figure IV-2.- Telemeter format.

The telemetry format was a time-division multiplex scheme wherein a series of subcarrier oscillators were sequentially pulsed on and off (fig. IV-2). Information was conveyed by the frequency of the pulse-gated subcarrier oscillator, by the duration of the pulse, and by the spacings between pulses. The signal consisted of 16 subcarrier oscillator pulses for a total of 48 channels of information for each telemeter.

The two telemeters were constructed as independently as was possible in order to improve overall system reliability. Separate solar cells and batteries were used to supply power as well as separate electronics for handling the data. A common antenna system was used for the two telemeters, but the two telemeters were connected through a hybrid junction so as to be electrically isolated. The sensors were divided into two groups as nearly equal as possible and telemetered separately. Each sensor was connected to only one telemeter, but the division was made so that sensors of the same type and sensitivity were equally distributed between both telemeters. This meant that if one telemeter failed, the experiment was not lost but that the exposed area was halved. A block diagram of the telemetry system is presented in figure IV-3 and the pertinent characteristics in table IV-1. The telemetry system consisted of three major units: An "A" telemeter, a "B" telemeter, and a radio beacon.

Telemeters: The "A" and "B" telemetric assemblies were quite similar and consisted of:

1. One signal conditioning module each
2. One encoder module each
3. One 16-channel subcarrier oscillator module each
4. One events-counting and storage module in the "A" assembly and two in the "B" assembly
5. One impact-detector amplifier and wave-shaper module each
6. One transmitter and diplexer module each
7. One secondary Ni-Cd battery module each
8. One command receiver and turnoff timer module each
9. One regulated dc-dc converter each

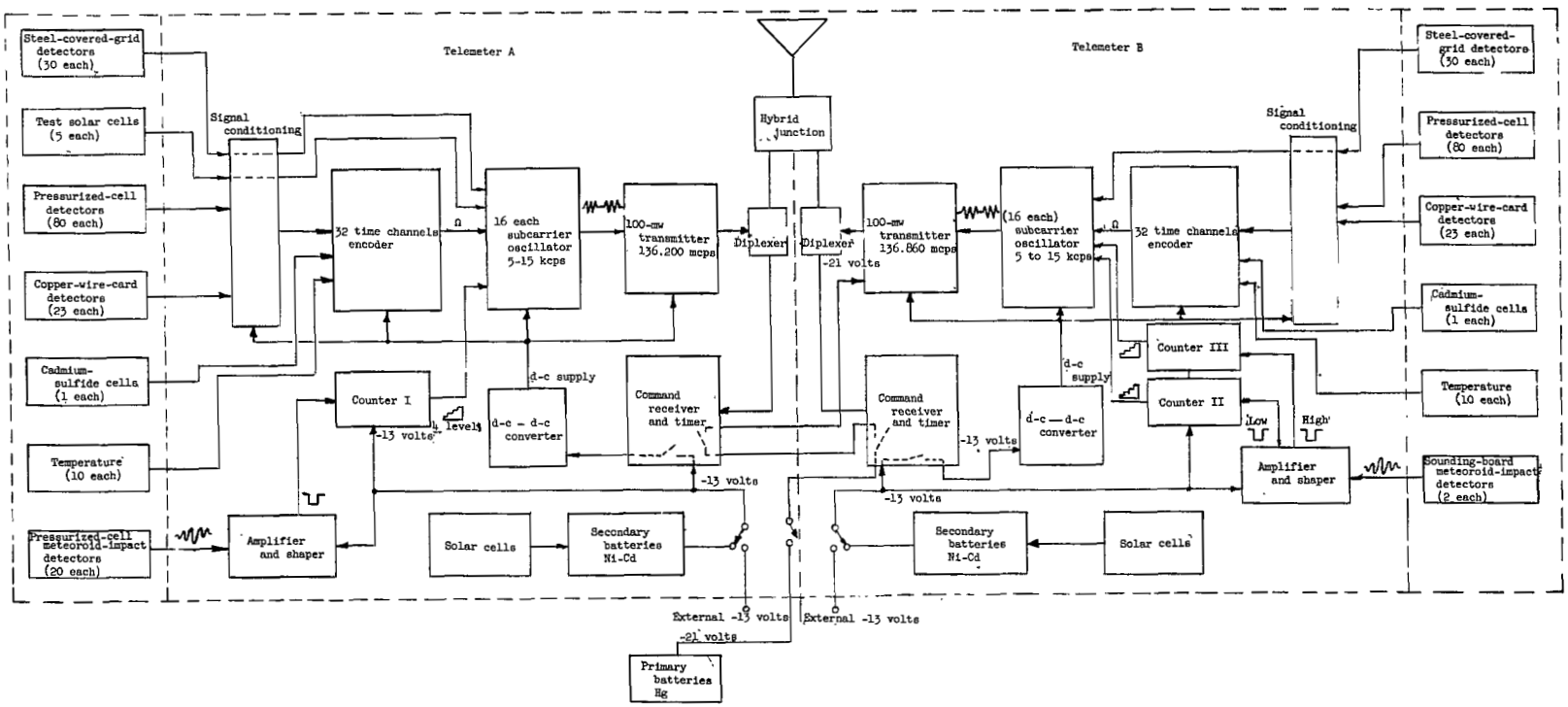

Figure IV-3.- Block diagram of telemetry system.

The command receivers, the microphone amplifiers, and the counters were continuously energized. Upon reception of an interrogation command, the dc-dc converters were energized and in turn furnished power to the encoders, the subcarrier oscillators, and the transmitters. The encoders then sampled each sensor approximately three times per second and generated a telemetry signal which then amplitude modulated the transmitters. After a 1-minute interval, the dc-dc converters were deenergized by the internal timers. The turnoff timers were not synchronized so the turnoff times did not necessarily coincide.

Radio Beacon.- The radio beacon consisted of the "B" telemeter transmitter module (item 6) and two primary (Hg) battery packs. The radio beacon had its power turned on prior to launch and was to transmit until its primary batteries were exhausted (about 1 week). Its power was routed through interlocks in the "A" and "B" command receivers so that it was silenced during interrogation of either telemeter (fig. IV-3). This override feature allowed for interrogation of the telemeters while on the launch pad for checkout purposes and during flight for readout purposes.

Telemetry Construction.- All modules except for the transmitter, batteries, and dc-dc converter were constructed on a printed circuit board and potted with a foam-in-place polyurethane potting resin. The transmitter was constructed on an aluminum chassis and potted with the polyurethane resin. The Ni-Cd battery module was potted with epoxy for added strength. The potting material was used to obtain the final module shape 5.50 inches in diameter and 1.00 inch high. The dc-dc converter was constructed on an aluminum chasis and had an aluminum case for added rigidity. The modules were stacked one upon another and the seven (eight for the "B" telemeter) module stack mounted upon a base containing the entrance plugs and associated wiring. Two 1/4-inch rods were run through the modules to bolt them to the base and a heavy walled canister was placed over them to give the modules the required strength and rigidity. The dc-dc converter was placed in the underside of the base and covered. Hermetically sealed connectors were used for entering the telemeters and all mechanical interfaces were sealed by using "O" rings. The telemeters were then pressurized to 20 psia. Figure IV-4 is a cutaway view of the "B" telemeter showing the construction methods and figure IV-5 is a photograph of the "A" telemeter with the canister removed. The thermal-design factors which apply to the telemeters

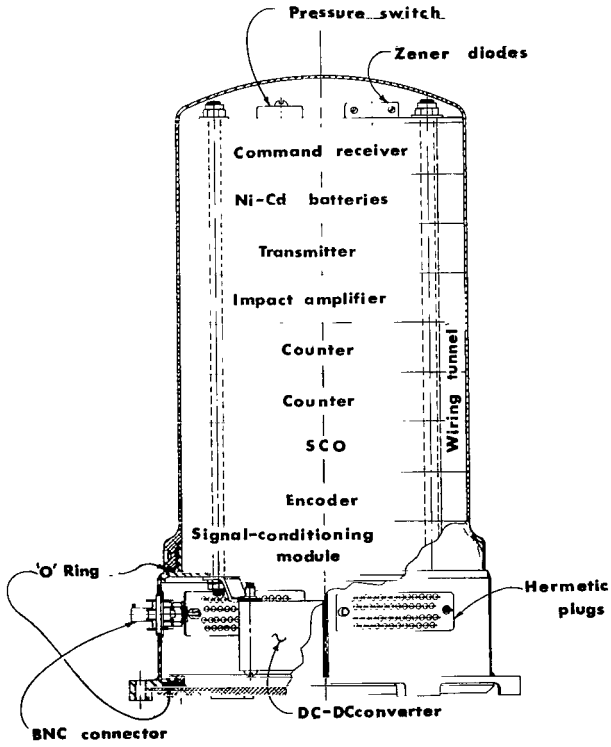

Figure IV-4.- Cut-away view of telemeter B assembly.

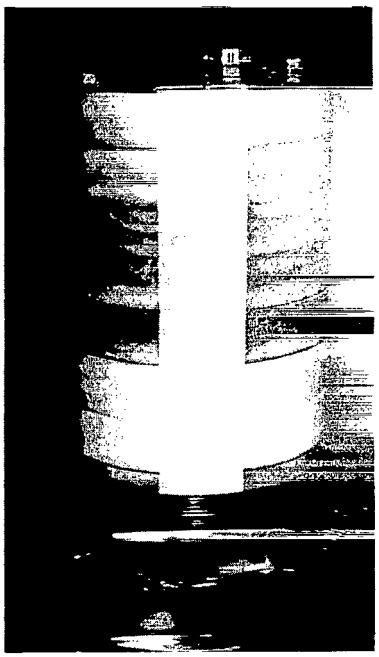

L-62-1572
Figure IV-5.- Telemeter A assembly.

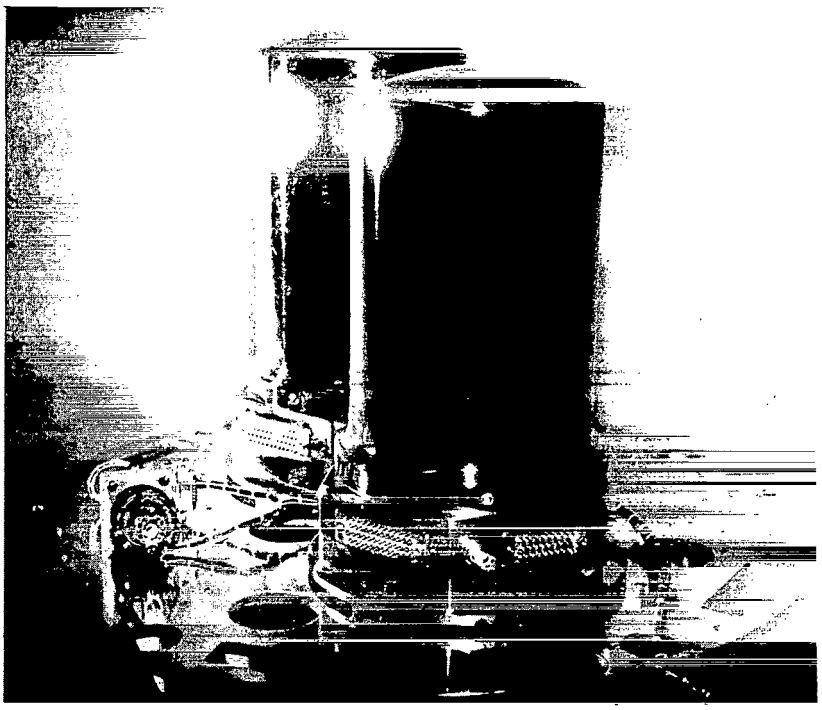

L-62-1568
Figure IV-6.- Telemetric assemblies on fiber-glass bulkhead.

are covered in Chapter VI. Figure IV-6 shows the "A" and "B" telemeters mounted upon a fiber-glass bulkhead.

Encoding System.- The function of the encoding system is to sample the various sensors sequentially and to generate a signal suitable for telemetry. The encoding system is composed of three subassemblies; each subassembly consists of a signal conditioning module, an encoder module, and a subcarrier oscillator (SCO) module. The signal conditioning module accepts inputs from the various sensors and operates upon them to form inputs acceptable to the encoder module and the subcarrier oscillator module. Section IV of this chapter on "Channel Allocations" presents a discussion of these procedures. The encoder module accepts its inputs from the signal conditioning module and generates a nonsynchronous pulse-duration modulation (PDM) wave train. The SCO's accept their inputs from the signal conditioning module and generate frequencies which are determined by their inputs. The SCO's are sequentially gated on and off by the PDM and other wave trains from the encoder and their outputs are summed into a common signal line. Only one subcarrier oscillator is gated on at any time.

Encoder Module.- The encoder circuitry consists of a timing multivibrator in a Royer circuit (ref. IV-2) for generating the duration and space times, a solid-state commutator for switching in the proper sensors, and a scale of 16 matrix for control purposes. Figure IV-7 shows the encoder, and circuit diagram 1 (at the end of this chapter) is a schematic of the encoder. Transistors Q_{33}, Q_{34}, and the timing multivibrator transformer comprise the timing multivibrator; Q_1 to Q_{32} comprise the solid-state commutator; Q_{35} to Q_{39} supply

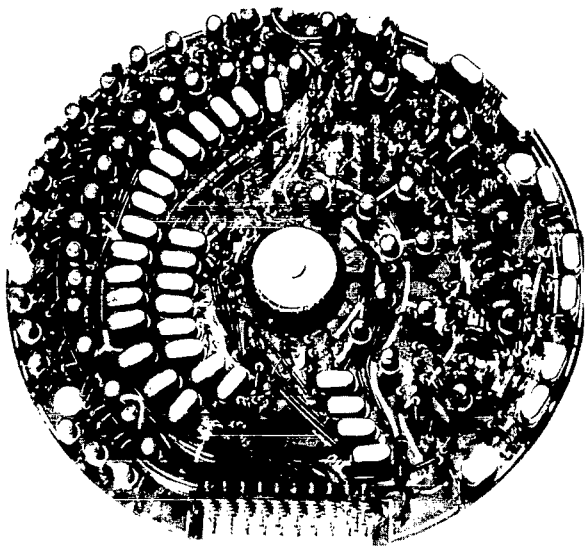

L-60-3770

Figure IV-7.- Forty-eight channel encoder module.

gating for the SCO module; Q_{40} to Q_{59} comprise the scale-of-16 counter; and Q_{60} to Q_{87} comprise the matrix which supplies gating pulses to the solid-state commutator and to the SCO module. Figure IV-8 is the timing diagram for the encoder and shows the relationship of the various waveforms. Note that the sync starts on S16 rather than on D1 and that all base gates start concurrently with a space start and step to the next base gate concurrently with spaces; that is, base gate A occurs for S16 and D1, base gate B occurs for S1 and D2, and so forth. This scheme was necessitated by the subcarrier oscillators. The scale-of-16 counter and matrix was driven from the oscillator gating and suffered a propagation delay of about 5 microseconds. If the commutation had occurred at the beginning of a duration, the wrong oscillator would be gated on during this 5-microsecond delay and would have distorted the leading edge of the duration burst. Commutating at the beginning of a space allowed up to 4 milliseconds for switching the subcarrier oscillators.

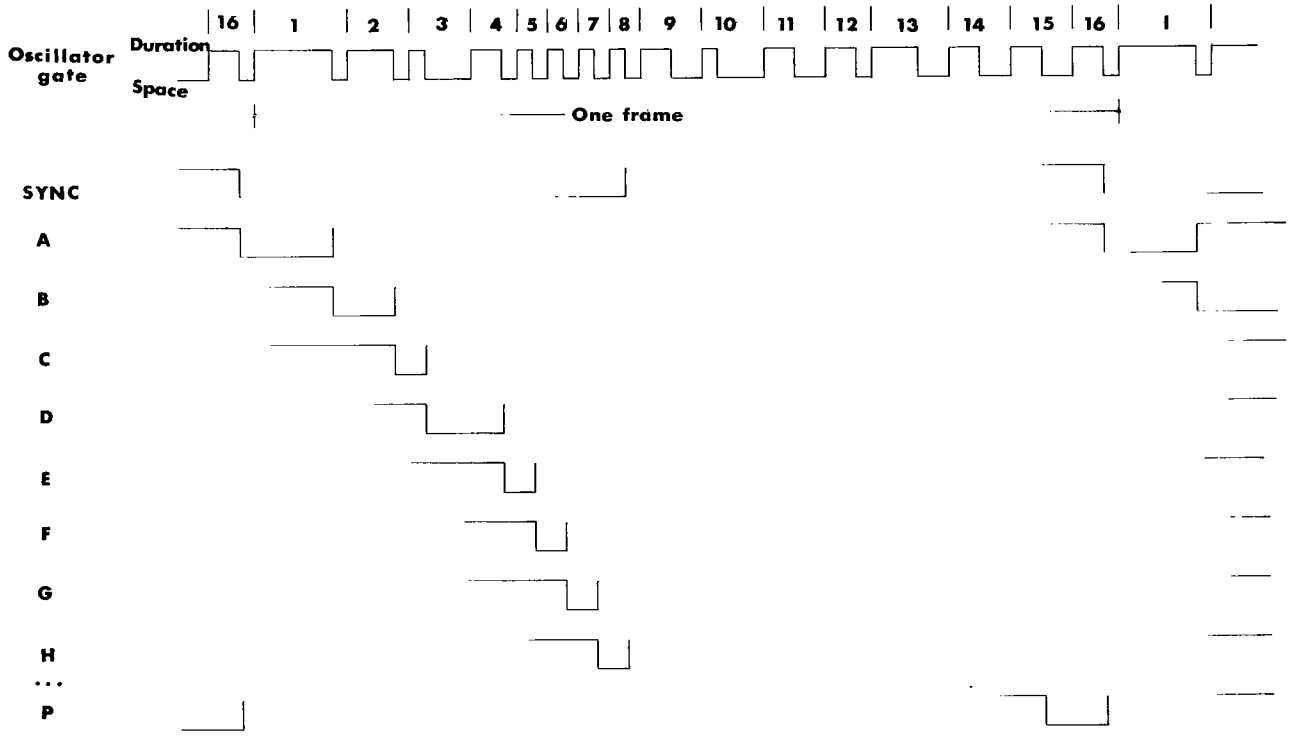

Figure IV-8.- Encoder timing diagram.

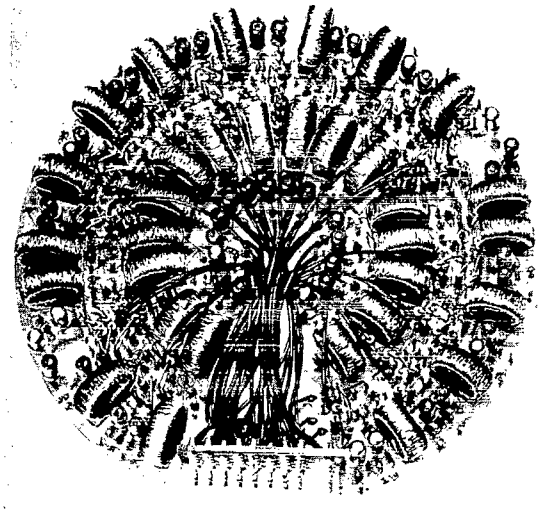

L-60-3768
Figure IV-9.- Subcarrier oscillator module.

Subcarrier Oscillator Module.- The subcarrier oscillator module (fig. IV-9) consisted of 16 identical subcarrier oscillators. These oscillators accepted their inputs from the signal conditioning module and their gate signals from the encoder. The SCO's were sequentially gated on by the encoder and their outputs summed onto a common signal line. Since the oscillator gating was time-division multiplexed, one signal only was present at any one time.

The basic subcarrier oscillator (circuit diagram 2) consists of a magnetic multivibrator in a Royer (ref. IV-2) circuit. The theory of operation is the same as for the timing multivibrator in the encoder; Q1 and Q2 and switching transistors and are either saturated or nonconducting. Core 1 and core 2 were tape wound with a square loop material. Transistor Q3 and core 2 form an inductive voltage absorber that varies the effective voltage across core 1, and therefore the switching frequency of core 1. The output was a square wave and was fed to the modulator. Blocking diodes were used in the output lines so that the 15 "off" subcarrier oscillators would not load down the "on" subcarrier oscillator. The absence of filtering or charging circuits permitted the SCO to be gated on and off and to become stabilized within one-half cycle of operation.

Counter Module.- The events-counting and storage system accepted pulses from the impact-detector amplifiers, counted these pulses, and generated output levels suitable for the subcarrier oscillators. The counter consisted of 12 complementary flip-flops connected in cascade which gave the unit a total-count capacity of 4,096. The counter did not have reset capability since nondestructive readout was a requirement of the system telemetry. With the application of the 4,096th pulse, the counter cycled and began counting anew. The outputs of the counters were weighted and summed so as to form octonary numbers. Four of these numbers modulated the subcarrier oscillators. The units are shown in figure IV-10 before potting; the impact-detector amplifiers are described in Chapter XII.

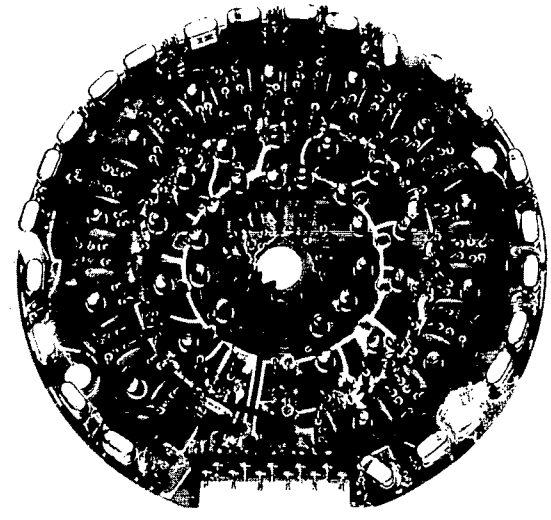

L-60-3767
Figure IV-10.- Events-counting and storage system.

A schematic of the complementary flip-flop (ref. IV-3) used in the events-counting and storage system is shown in circuit diagram 3. One NPN and one PNP transistor conduct in each of the two states of the flip-flop, either Q1 or Q3 or Q2 and Q4. This method of two-transistor regeneration gave a circuit gain of beta squared and thus allowed operation at a power level of less than 1 milliwatt. The steering transistor, Q5, conducted only during switching. The application of a 2-volt negative-going pulse switched the flip-flop and thus the polarity of the voltage across Q5. Transistor Q5 was chosen so as to have gain in the normal and inverted configurations.

The interconnections of the 12 flip-flops are shown in the events-counting and storage-block diagram (fig. IV-11). The 12 flip-flops were divided into two equal groups of six each and stacked to operate from the available -13-volt power supply. The outputs contained a common mode voltage which was bucked out in the subcarrier oscillator inputs.

Transmitter Module.- The transmitters were of the master-oscillator power-amplifier type wherein the oscillator was crystal stabilized at the output frequency and the final amplifier was base modulated. The transmitter provided a minimum carrier output through the diplexer of 100 milliwatts at a collector supply of -21 volts d-c. Modulated output was typically 150 milliwatts. Total transmitter input was 750 milliwatts which gave an efficiency of 20 percent.

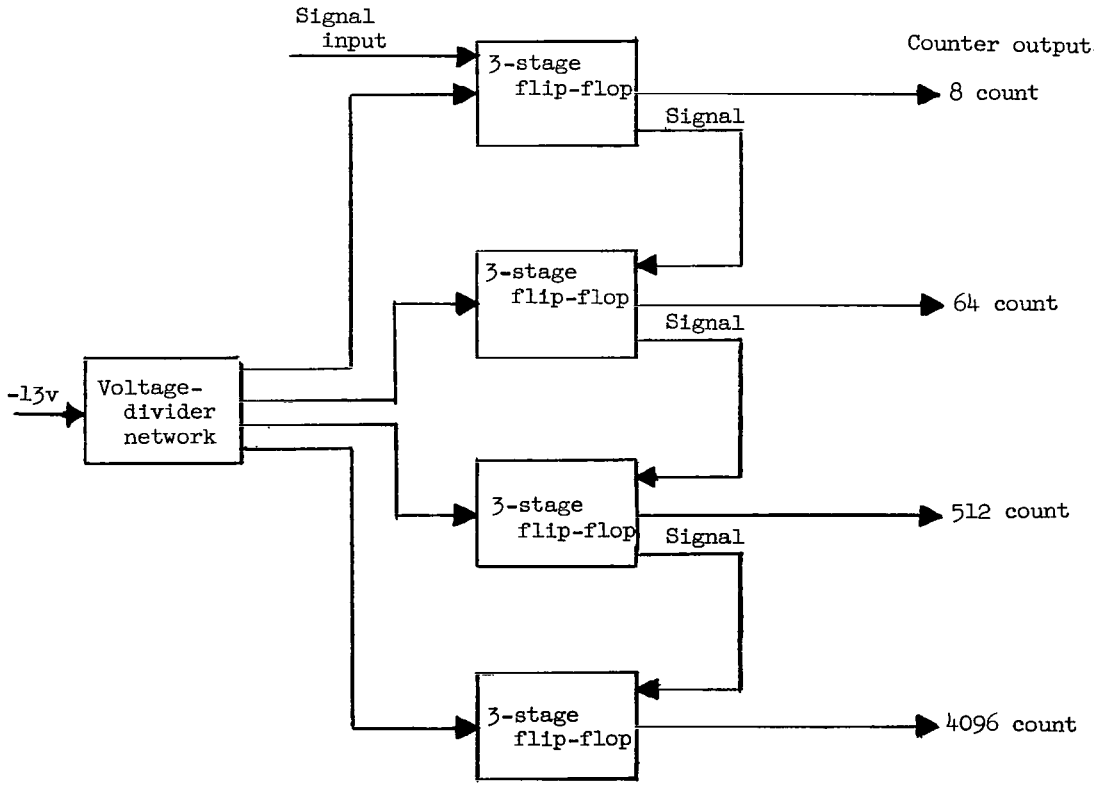

Figure IV-11.- Counter-module block diagram.

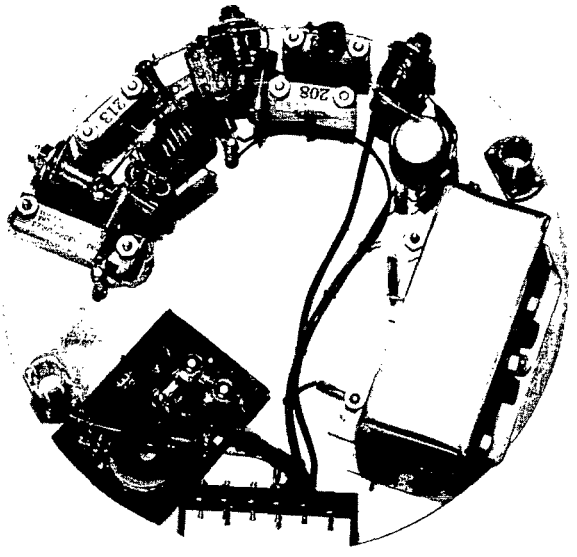

L-60-3769
Figure IV-12.- Transmitter module.

The transmitter is shown in figure IV-12 and the transmitter schematic is shown in circuit diagram 4. Transistor Q1 and associated circuitry compose the crystal stabilized oscillator; Q2, Q3, and associated circuitry compose the base-modulated power amplifier; Q4, Q5, and associated circuitry compose the modulator; L6, L7, C15, and C19 compose a frequency-selective diplexer. This diplexer serves the dual purpose of routing the telemetry rf (radio frequency) signal from the transmitter to the antenna and the command receiver rf signal from the antenna into the command receiver.

The modulator was a saturating (clipping) type wherein the output amplitude was constant so long as the input remained above a threshold level. This type of operation necessarily resulted in a square-wave output. Sine wave or linear operation could have been used with a more complex form of amplitude stabilization. An examination of the spectrum of a square wave reveals an infinite series of harmonics. Stated mathematically, the Fourier series is:

$$e(t) = E\frac{4}{\pi}\cos \omega t - E\frac{4}{3\pi}\cos 3\omega t$$

$$+ E\frac{4}{5\pi}\cos 5\,\omega t - \cdots$$

A typical transmitted spectrum is shown in figure IV-13 which shows both the A and the B telemeter spectra. Theoretically, there should be more than 2-percent crosstalk even with a 660-kcps spacing, but bandwidth limitations in the modulator and in the final tank circuit kept the crosstalk well below 0.1 percent. Modulating and detected waveforms are shown in figure IV-14. The detected waveforms were taken by using a receiver with a 50-kcps bandwidth.

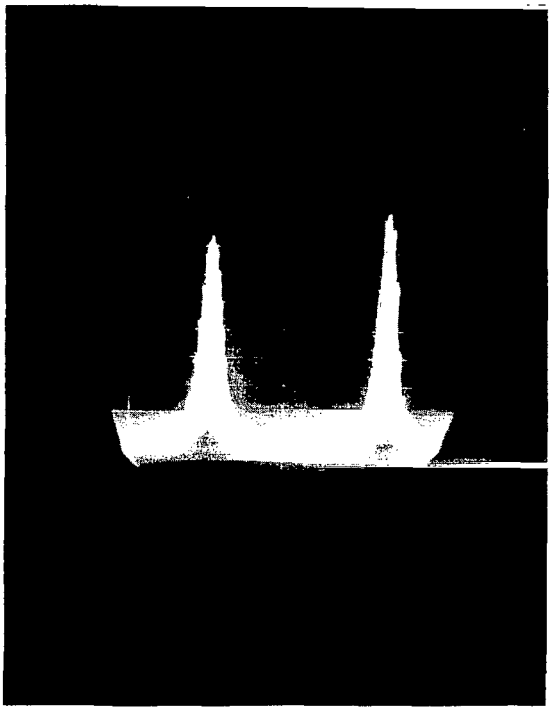

Figure IV-13.- Transmitted spectrum. L-64-3087

Command Receiver Module.- The command receivers (fig. IV-15) used in Explorer XIII were similar to those used in Vanguard II and III (ref. IV-4). The major changes were to update components and to add a 1-minute turn-off timer. In

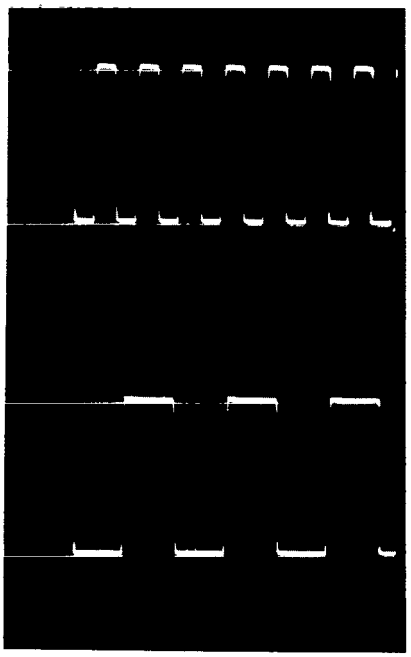

15 kcps

5 kcps

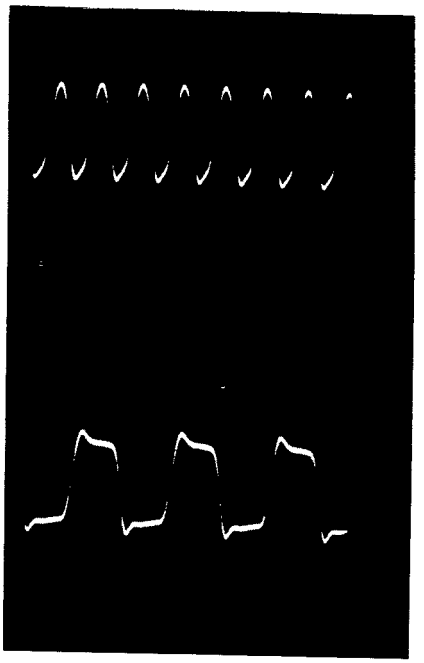

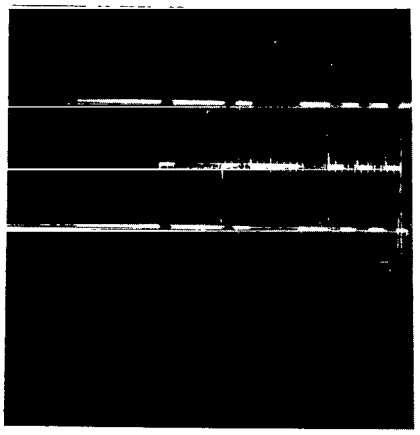

Duration - space waveforms

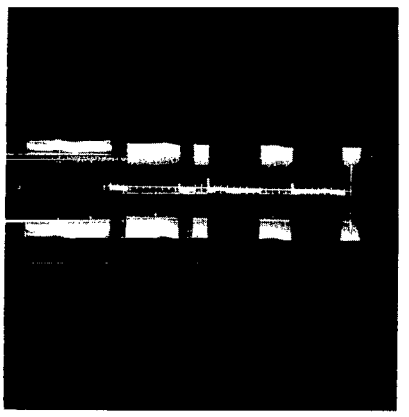

Modulator waveforms

Receiver waveforms

Figure IV-14.- Modulation waveforms.

L-64-3088

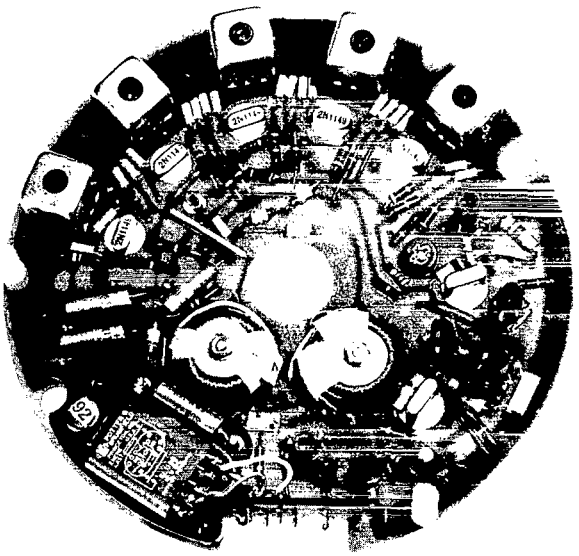

L-60-3772
Figure IV-15.- Command receiver module.

order to increase the reliability of the system, it was decided to accomplish data readout by using only one ground action; that is, the satellite telemeters were turned on by a ground command, the telemeters transmitted their data, and then automatically turned themselves off after about a 1-minute interval without requiring an additional ground action.

The command receivers were double-conversion superheterodynes and were fixed tuned to one command frequency. As shown in circuit diagram 5, the first and second converters Q1 and Q2 were crystal stabilized in order to obtain the required frequency stability. The second intermediate frequency (i.f.) amplifiers (Q3 to Q6) provided the major portion of the system gain (over 100 decibels). The i.f. stages were single-tuned transformer coupled and provided a bandwidth of 20 kcps between the 3-decibel points. Transistor Q7 and associated circuitry formed a "weak-signal" detector; L12, L13, C50, C51, and C52 composed an overcoupled double-tuned filter with a 5-percent bandwidth; Q8, D5, and associated circuitry composed a peak-to-peak detector; Q9, Q10, and associated circuitry composed the relay amplifier. RE-1 is a dual-coil magnetic-latching relay. The relay was turned on by the command receiver and turned off by the interval timer. The interval timer was comprised of Q11, Q12, and Q13, and associated circuitry.

Dc-dc Converter.- The dc-dc converter furnished power to the encoder, subcarrier oscillators, and transmitter at the appropriate voltages. The output voltages were held to within plus or minus 1 percent over an ambient temperature range from -10° C to 60° C, with an input change of plus or minus 10 percent, and with a load decrease of 50 percent; this was accomplished with a conversion efficiency of 80 percent. The converter consisted of two units, a regulator and a dc-dc transformer in a Royer circuit (ref. IV-2). The dc-dc converter is shown in figure IV-16, and the dc-dc converter schematic is shown

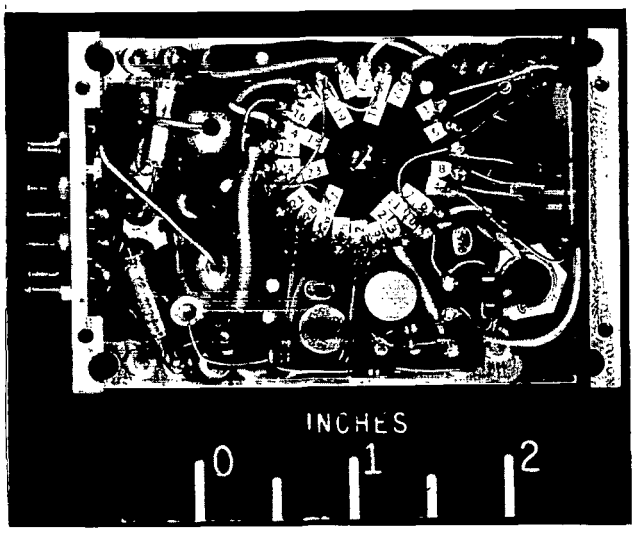

Figure IV-16.- Dc-dc converter. L-60-8607

in circuit diagram 6. Q1, Q2, Q3, D1, and D2 form a series regulator. Transistors Q4 and Q5 along with the square-loop core form the d-c-to-a-c converter and D3 and D12 supply the output voltages. Diodes D13 and D14 supplied bias for Q4 and Q5; this method of obtaining the switching-transistors bias made the dc-dc converter short-circuit proof.

SECTION III - ANTENNA SYSTEMS

Due to the initial spinning and the eventual tumbling modes of the satellite, an isotropic antenna system was a necessity. An additional requirement was that the antennas be stowable during the launch phase when the heat shields were on and that they automatically unfold when the heat shields were jettisoned. The mechanical design of this feature is covered in chapter III.

The selected antenna system consisted of four erectile monopoles spaced 90° electrically and 90° physically around the satellite body in a turnstile array. This type of antenna system provides circular polarization when viewing the satellite head on, linear polarization when viewing broadside, and circular polarization of the opposite sense when viewing tail on. Since weight considerations necessitated utilizing the same antenna system for transmission from and reception at the satellite for both telemeters, a hybrid junction (ref. IV-5) was used to tie the telemeters to the antenna system while still isolating them. A frequency-selective diplexer was used in each telemeter to separate the transmitters and receivers. The overall system is shown in the telemeter block diagram (fig. IV-3) and the hybrid-junction turnstile antenna system in figure IV-17.

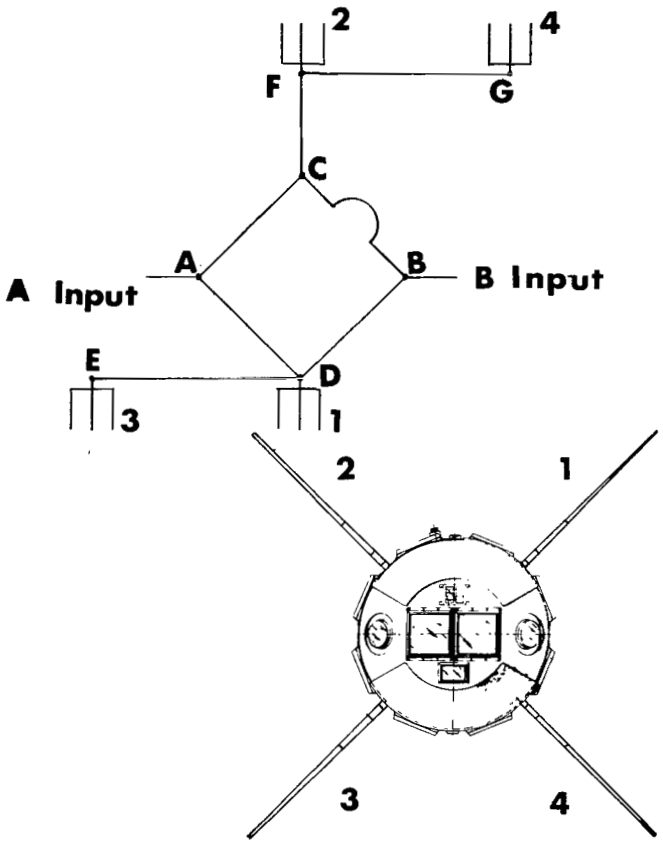

Figure IV-17.- Hybrid junction and turnstile antenna system.

The hybrid junction provides two isolated inputs and two isolated outputs with equal power division between the two outputs. The hybrid junction, when terminated in a resistive 50-ohm load, is capable of maintaining a 40-decibel isolation between inputs and a power division equal to ±1 decibel between outputs over a 4-percent frequency range. The hybrid-junction turnstile antenna system was usable over a 20-percent frequency range.

The operation of the hybrid junction may be understood by noting that there are two paths from point A to point B (ACB and ADB) and by noting that the distances are unequal by one half wavelength or 180 electrical degrees. Assuming proper operation, the signal through path ACB will arrive 180 electrical degrees later than the signal through ADB and they will be in counterpoise. The net result is that the power at point B due to that at A is zero. The inverse process from B to A is analogous. The phasing of the turnstile array may be understood by noting the line lengths from the inputs to the individual monopoles. The lines DE and FG are one half wavelength each and are used to connect monopoles 1 and 3 (2 and 4) together as dipoles. Monopoles 1 and 3 (2 and 4) are diametrically opposed and the two dipoles are in quadrature. The line lengths from point A to the monopoles 1, 2, 3, and 4 are 1/4, 1/2, 3/4, and 1 wavelength so that the signals are electrically spaced by 90°. Therefore, the resulting voltage maxima rotate. It should be noted that the line lengths from point B to the monopoles 1, 2, 3, and 4 are 1/4, 1, 3/4, and $1\frac{1}{2}$ wavelengths so that the voltage maxima occur in the opposite rotating sense.

Since the system is passive in nature, the inputs and outputs may be interchanged without affecting system operation. This allows both transmission and reception through the hybrid junction and antenna system. The antenna patterns for the spinning and tumbling modes are shown in figures IV-18 and IV-19, and VSWR is shown in figure IV-20.

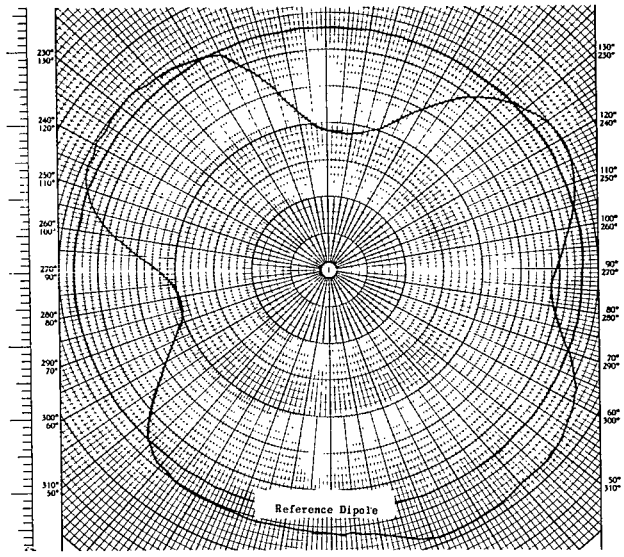

Figure IV-18.- Antenna pattern for a spinning satellite; stable mode.

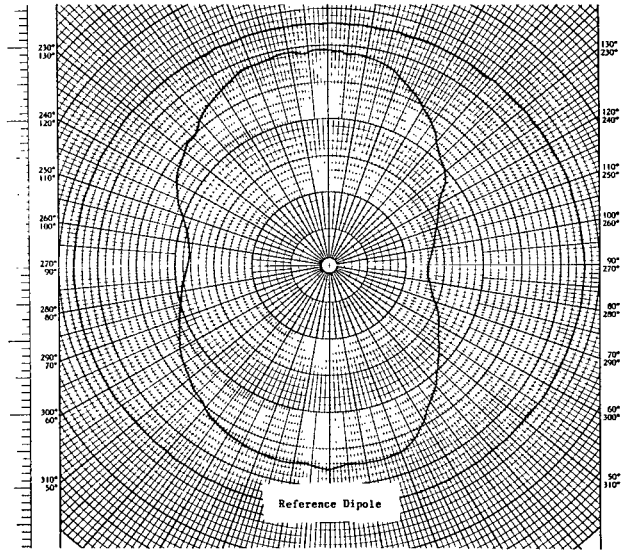

Figure IV-19.- Antenna pattern for a tumbling satellite; tumbling mode.

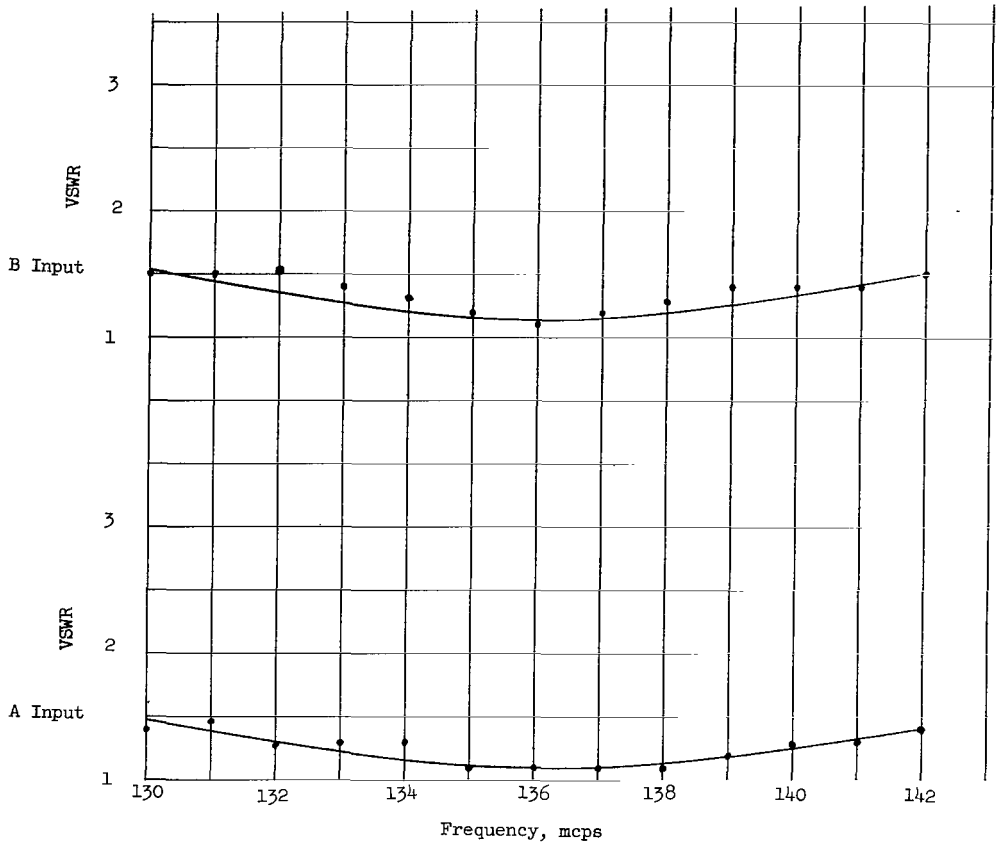

Figure IV-20.- Voltage standing wave ratio.

SECTION IV - CHANNEL ALLOCATIONS

In order to make efficient utilization of channel capacity, it was necessary to obtain a complete knowledge of the environment to be measured as well as a thorough understanding of the sensors. Only when this is done, could the telemetry system be used to its fullest advantage. As is true of all telemetry systems, the telemetry system for Explorer XIII exhibited several peculiarities which had to be designed around. The most evident of these was the crosstalk or hysteretic effect which preceding time channels had on the succeeding time channels. This effect was minimized by grouping sensors according to their measurements so that adjacent channels were functions of the same inputs, that is, the channels were grouped so that the crosstalk effects were minimized.

The inputs to the telemetry system were of two types: a voltage input to the subcarrier oscillators (frequency channels) and a resistance input to the timing multivibrator (time channels). The inputs to the frequency channels were high impedance (approximately 100 K) and the inputs to the time channels were low impedance (a maximum of 5,000 ohms). The inputs to the frequency channels were double ended and were of the type wherein common mode voltages could be bucked out. The inputs to the time channels were also double ended but were of the type that required the sensor to be isolated from ground.

The sensors to be used in any experiment may be categorized into two types: analog, where the output may take any value between two end points; and digital, where the output has only a discrete and finite number of steps. In general, when using an analog telemetry system, the analog sensors require a complete channel for telemetry while the digital sensors may be grouped several to a channel. The digital data may be grouped in two different ways: as combinations, wherein one knows when an event occurs but does not know which one of the n possible events has occurred; and as permutations, wherein one not only knows when an event occurs, but which event of the n possible events has occurred.

An examination of the digital data showed that there were only two types, penetration and impact. A scrutiny of the penetration data revealed that not only were permutations unnecessary, but that the desire to expose all sides of the satellite equally made combinations practically a requirement. Accordingly, the penetration data were telemetered as combinations and the placement of the sensors was distributed so as to give an isotropic view of space. The impacts, being scaled for storage, were weighted and therefore required treatment as permutations. In the signal conditioning process, the first assumption was that the aggregate telemetry system was capable of an accuracy not better than ±5 percent of full scale. Accordingly, all digital data were encoded so that each step was approximately 10 percent of full scale. It should be noted that few telemetry systems are capable of much better accuracy from the sensor to the final data listings.

A puncture of the pressurized-cell detectors resulted in a switch opening. The output of this switch was an on-off action which readily lent itself to signal conditioning. Using the ±5-percent resolution criterion, 10 cells were encoded onto each channel as combinations which give 16 channels of information. Sixteen time channels were used for the telemetry, 8 on the "A" system and 8 on the "B" system. The cells in each channel were laid out in two rows of 5 cells each with two rows placed diametrically opposite so as to sensitize both sides of the spacecraft. Because of the nature of the detectors, a temperature correction was not required for the raw data. The final channel allocations are shown in table IV-2 and in figure IV-21; the detector layout is shown in figure IV-22. The signal conditioning is shown in figure IV-23 along with the resulting resolution.

Penetration of the steel-covered-grid detector by a micrometeoroid broke a gold grid. This breaking of continuity was the telemetered data. Reference 6 gives a detailed description of the sensor and the fabrication techniques. Again, using the ±5-percent resolution criterion, the foil gages were encoded onto the frequency channels to give eight bits of information per channel. This signal-conditioning scheme along with the ensuing resolution is shown in figure IV-24. (See ref. IV-6 for the actual sensor grouping and location.) It should be noted that the incompatibility of the high internal impedance of the foil gages and the low input impedance of the time encoding circuitry precluded efficient utilization of available time channels. At best, only three bits could have been placed on one time channel. Due to the swamping action of the current-limiting resistors (fig. IV-24), the temperature effects on the sensors were minimized. Six frequency channels and four time channels were used for the telemetering, three frequency channels and two time channels each on the "A" and "B" telemeters. Table IV-2 and figure IV-27 show the final channel allocations.

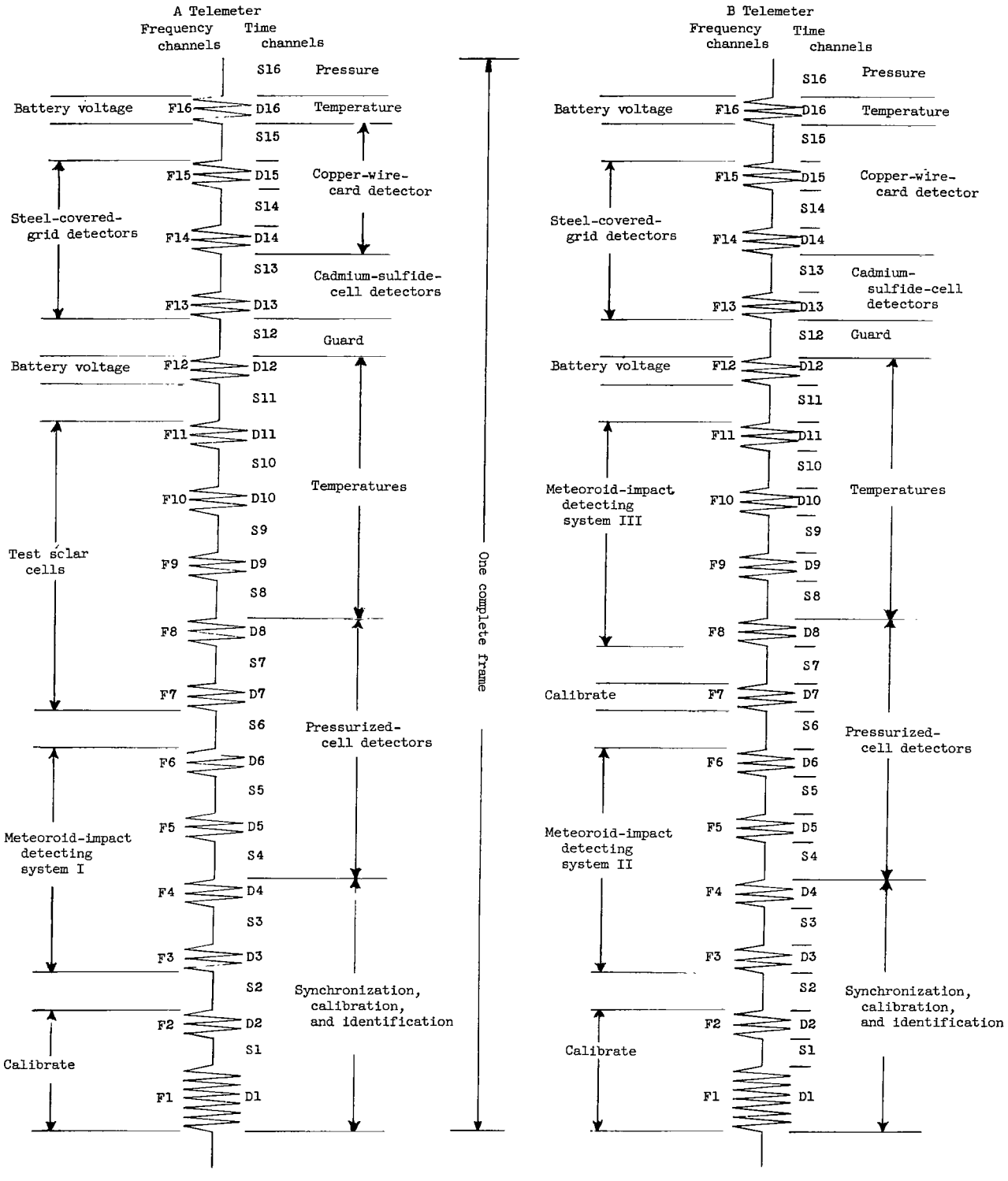

Figure IV-21.- Channel allocations.

The copper-wire-card detectors were melamine cards closely wound with copper wire. A micrometeoroid breaking the wire would cause the card to open. This interruption of continuity was the telemetered data. The signal-conditioning scheme is shown in figure IV-25 and the sensors are described in detail in chapter X. The channel allocations and the sensor layout are shown in figures IV-21 and IV-22, respectively. Ten time channels were used for telemetry, five each from the A and B telemeters.

The events-counting and storage system, which counted the pulses from the micrometeoroid-impact-detection system described in chapter XII, had as outputs octonary weighted voltage levels. These outputs had been treated as permutations and were conditioned as shown in figure IV-26. The channel allocations are shown in table IV-2 and in figure IV-21 and the microphone layout is shown in figure IV-22.

The temperature measurements located as described in chapter VI were made with thermistors, which are temperature-sensitive semiconductors having a large negative temperature coefficient of resistance. Four types of thermistors were used to cover four different temperature ranges. The types and their ranges are:

Thermistor	Temperature range, °C	Resistance at 25° C, ohms
GB25J1	-60 to 10	500
35A2	-10 to 60	5,000
38C2	0 to 70	8,000
GA42J2	10 to 100	20,000

It should be noted that the GB25J1 and the GA42J2 were used in conjunction to measure a temperature range from -60° C to 100° C. It can be shown that the thermistors have their maximum sensitivity at about 5,000 ohms and have end limits of about 500 and 50,000 ohms. Figures IV-27 to IV-29 show the temperature resolutions that were calculated for the 35A2, 38C2, and the GB25J1 - GA42J2 combination by using the criterion of ±5-percent telemetry resolution. Two complete sets of temperature measurements were made on the spacecraft and were diametrically opposed so as to indicate temperature gradients around the structure (one set was placed on each telemeter).

SECTION V - GROUND COMPATIBILITY TESTS

In order to insure compatibility between the orbiting satellite and the ground-receiving stations, the prototype telemeters were given an extensive series of tests at the NASA Goddard Space Flight Center (GSFC) and at Blossom Point, Maryland. The telemetry signals were demodulated by receiving equipment at GSFC and recorded on magnetic tape at various signal-to-noise ratios. This magnetic tape was then returned to the Langley Research Center where the recordings were read out and the results analyzed. The radio beacon signal

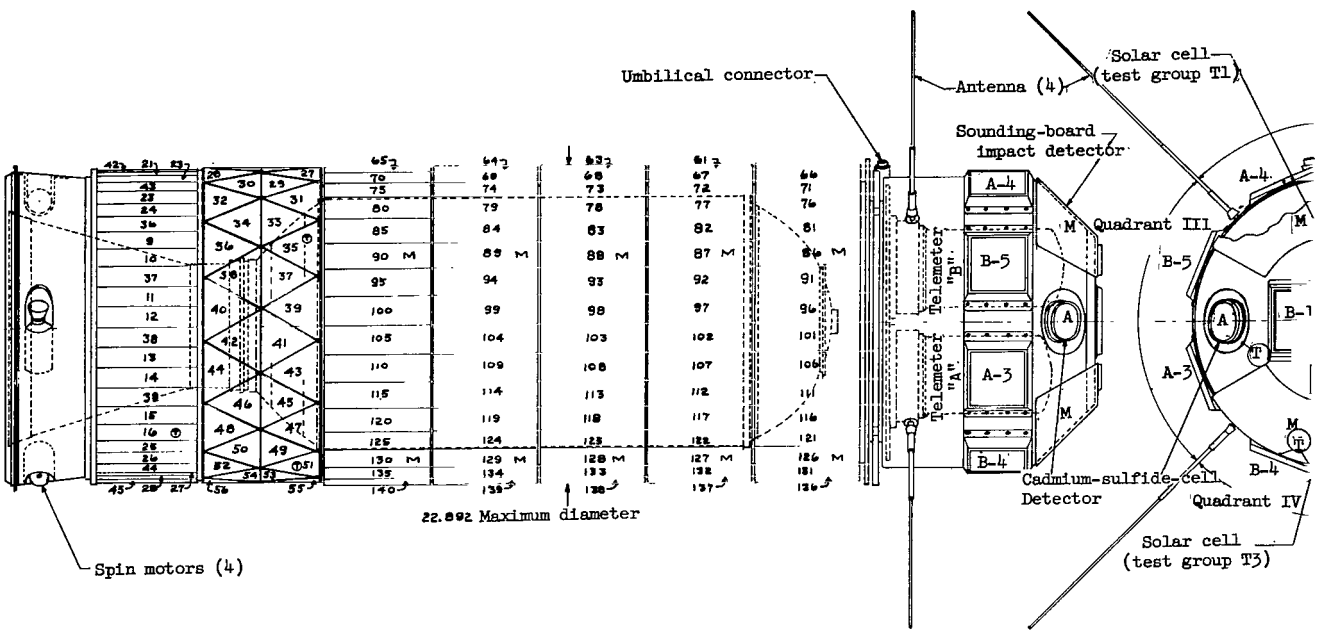

Penetrations	R, ohms	ΔR, ohms	Change, percent of full scale
0	0	---	---
1	470	470	9.4
2	940	470	9.4
3	1,410	470	9.4
4	1,880	470	9.4
5	2,350	470	9.4
6	2,820	470	9.4
7	3,290	470	9.4
8	3,760	470	9.4
9	4,230	470	9.4
10	4,700	470	9.4

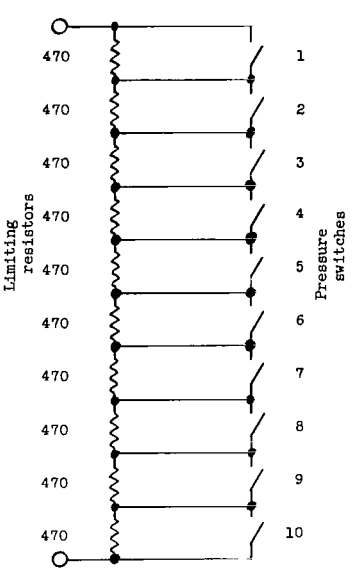

Figure IV-23.- Signal conditioning for pressurized-cell detectors. (R is limiting resistors.)

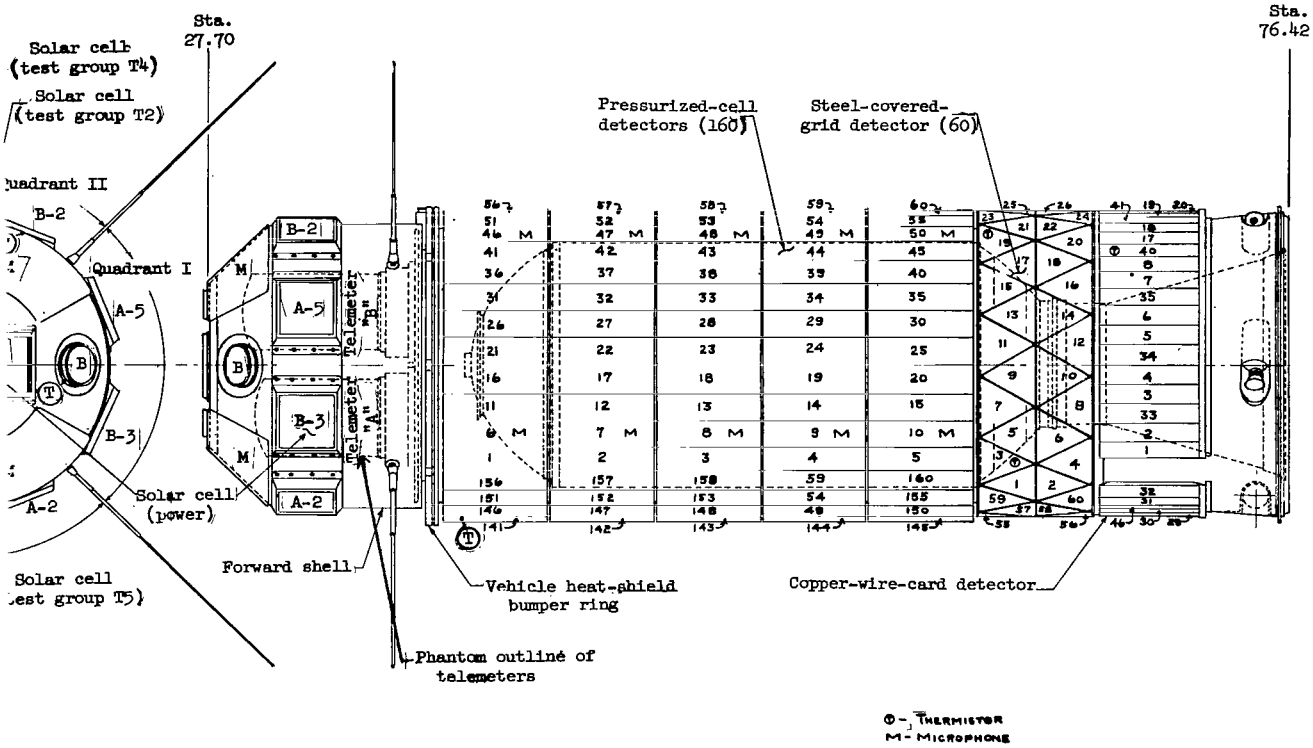

Figure IV-22.- Detector layout.

Penetrations	E_o, volts	ΔE_o, volts	Change, percent of full scale
0	2.737	-----	----
1	2.459	0.278	10.2
2	2.167	.292	10.7
3	1.857	.310	11.3
4	1.529	.328	12.0
5	1.182	.347	12.7
6	.812	.370	13.5
7	.419	.393	14.4
8	.000	.419	15.3

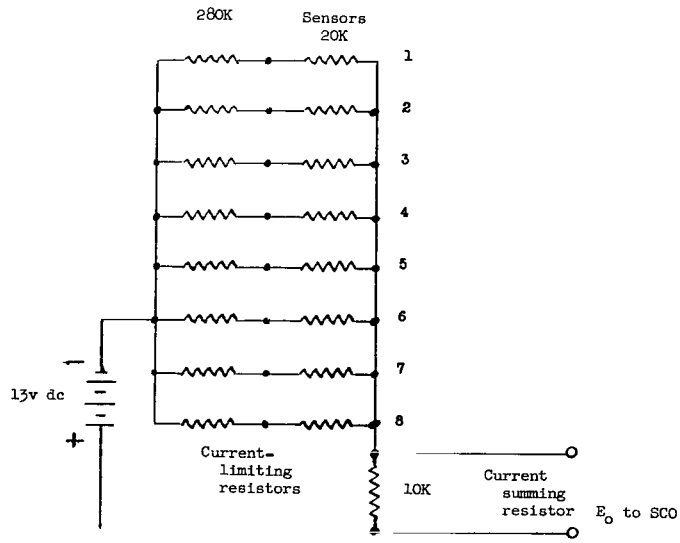

Figure IV-24.- Signal conditioning for steel-covered-grid detectors. (E_o is output voltage.)

Penetrations	R, ohms	ΔR, ohms	Change, percent of full scale
0	1,240	---	----
1	1,930	690	13.8
2	2,620	690	13.8
3	3,310	690	13.8
4	4,000	690	13.8

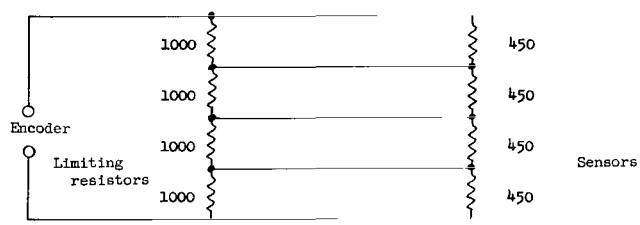

Figure IV-25.- Signal conditioning for copper-wire-card detectors.

Penetrations	25K	50K	100K	E_o Percent as f(E_{in})	Change, percent of full scale
0	0	0	0	0	0
1	0	0	1	14.3	14.3
2	0	1	0	28.6	14.3
3	0	1	1	42.9	14.3
4	1	0	0	57.1	14.3
5	1	0	1	71.4	14.3
6	1	1	0	85.7	14.3
7	1	1	1	100.0	14.3

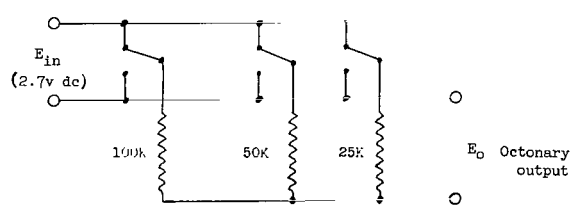

Figure IV-26.- Signal conditioning for impacts-counting and storage system. (E_{in} is input voltage.)

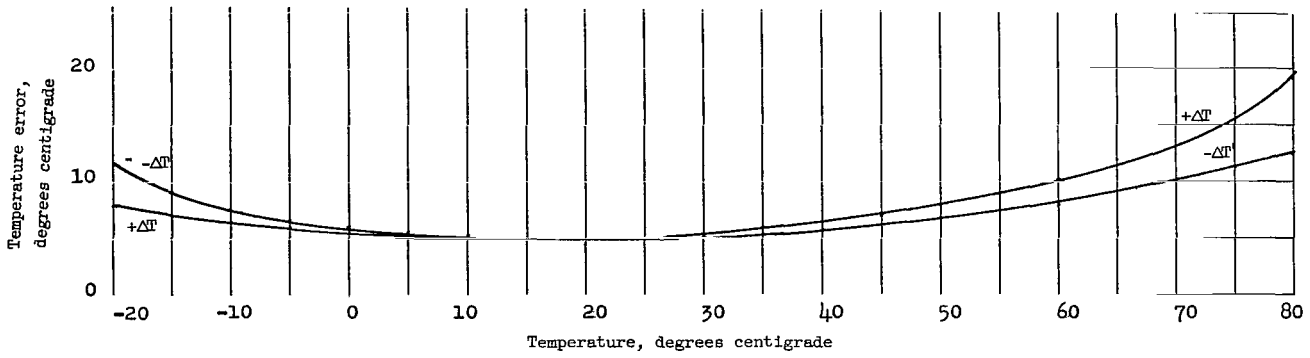

Figure IV-27.- Midrange temperature resolution for thermistor 35A2. (+ΔT is maximum up error in positive direction and -ΔT is maximum down error in negative direction.)

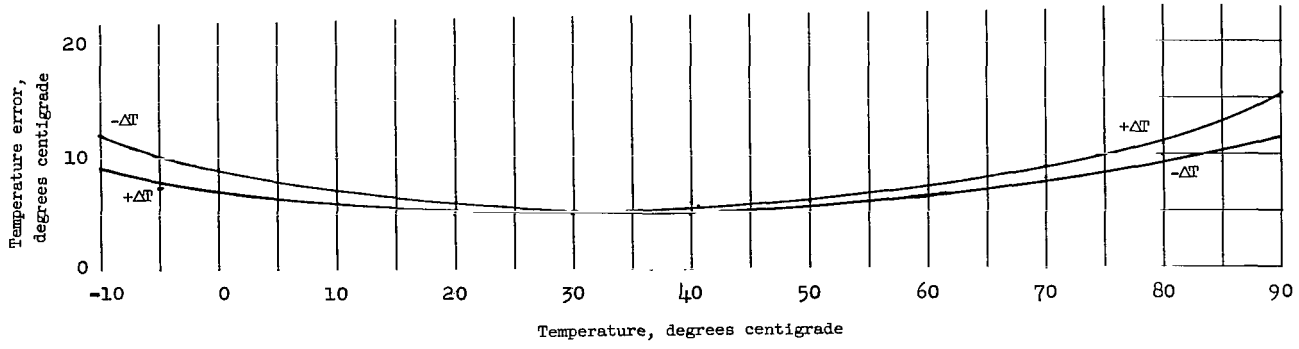

Figure IV-28.- Temperature resolution for thermistor 38C2.

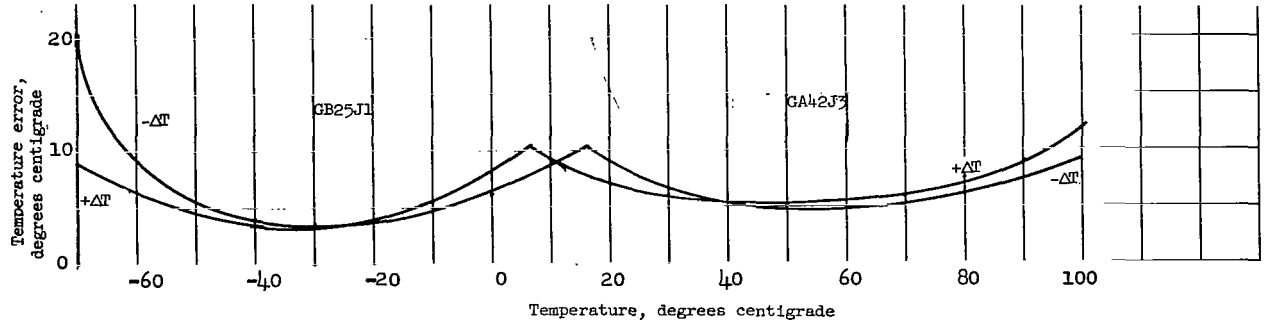

Figure IV-29.- High-low range temperature resolution.

was measured by the Minitrack Interferometer System and the results recorded on a strip-chart recorder. This record was analyzed by GSFC and LRC. The results of the tests showed that the two systems were entirely compatible.

The telemetry tests were conducted as shown in figure IV-30. The satellite electronics were placed in a shielded room to minimize rf leakage and the output at point A was adjusted by means of an attenuator to give 0 dbm carrier level. This signal was further attenuated to give inputs to the receiving system of various levels from -90 dbm down to -125 dbm. The modulation was recovered by means of an "auxiliary diode" and recorded on magnetic tape. The signals, as recovered, are shown in figure IV-31 for both the A and B telemeters. These tests did not include sky noise and therefore show signals about 4 decibels cleaner than were obtained operationally. The anticipated signal-to-noise ratios were shown in figure IV-1.

The tracking tests were conducted as shown in figure IV-32. The output at point A was again adjusted by means of an attenuator to give 0-decibel carrier level. This signal was further attenuated to give inputs to the tracking receivers of various levels from -80 dbm down to -130 dbm. The inputs to the

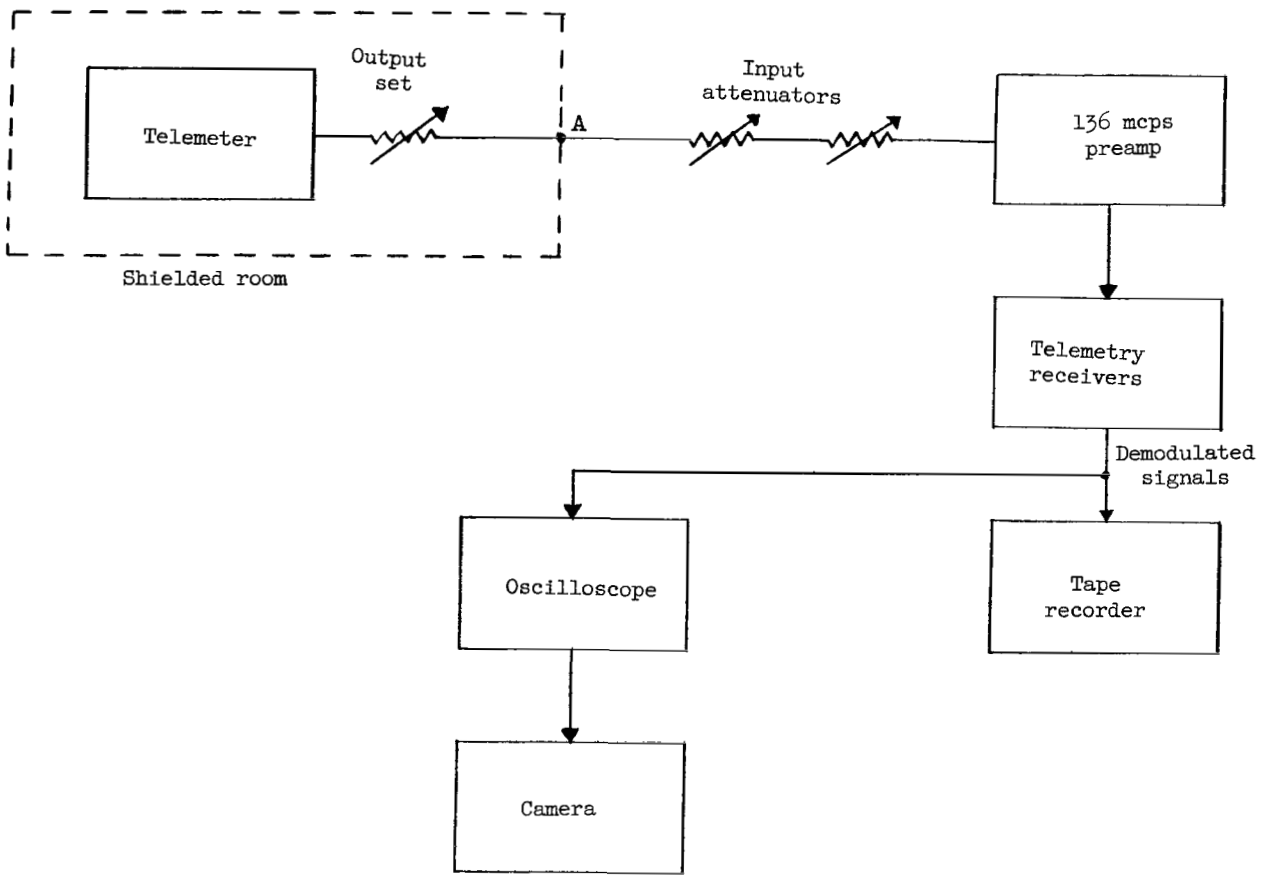

Figure IV-30.- Telemetry compatibility tests.

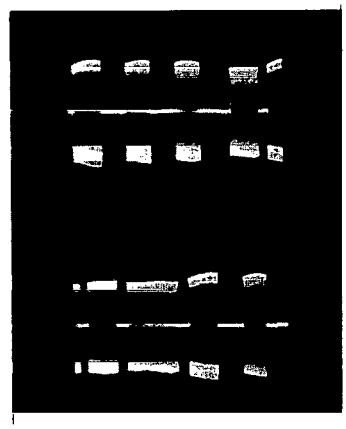

-90 dbm

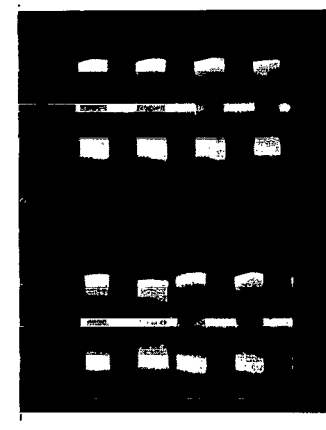

-100 dbm

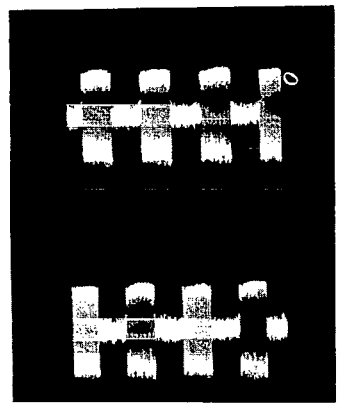

-110 dbm

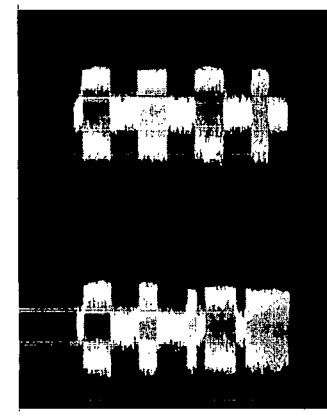

-115 dbm

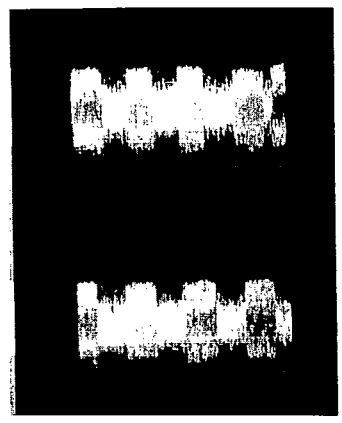

-120 dbm

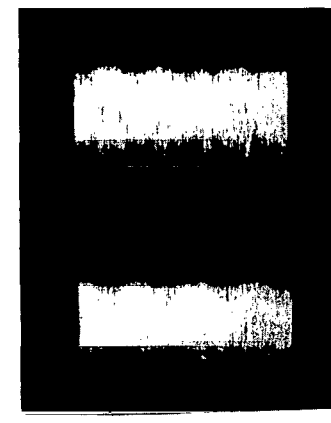

-125 dbm

(a) Telemeter 1-B. L-64-3089

Figure IV-31.- Demodulated telemetry signals.

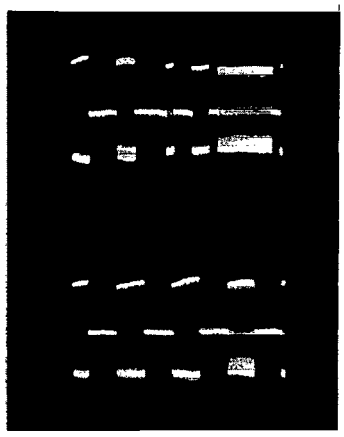

-90 dbm

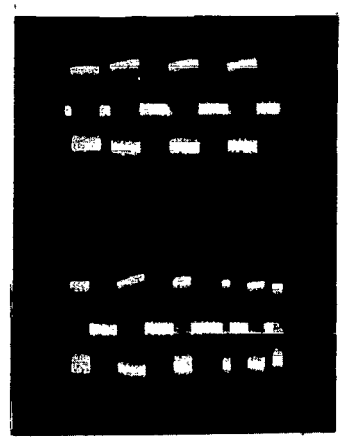

-100 dbm

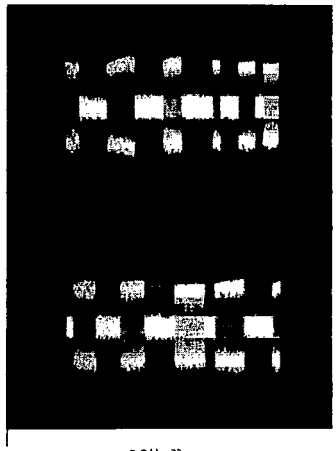

-108 dbm

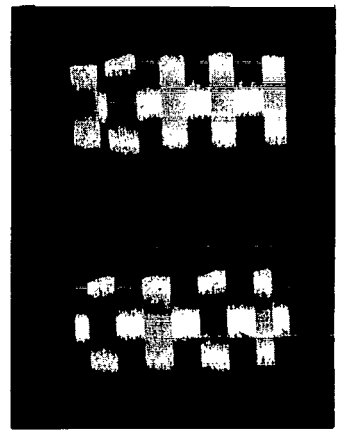

-110 dbm

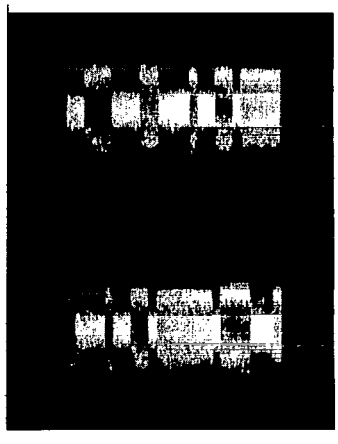

-115 dbm

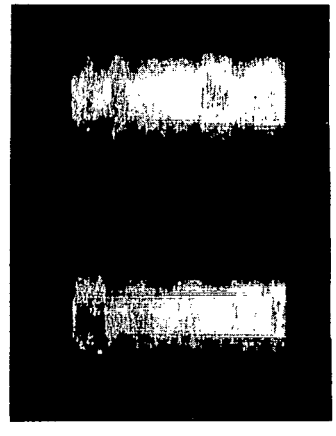

-120 dbm

(b) Telemeter 1-A. L-64-3090

Figure IV-31.- Concluded.

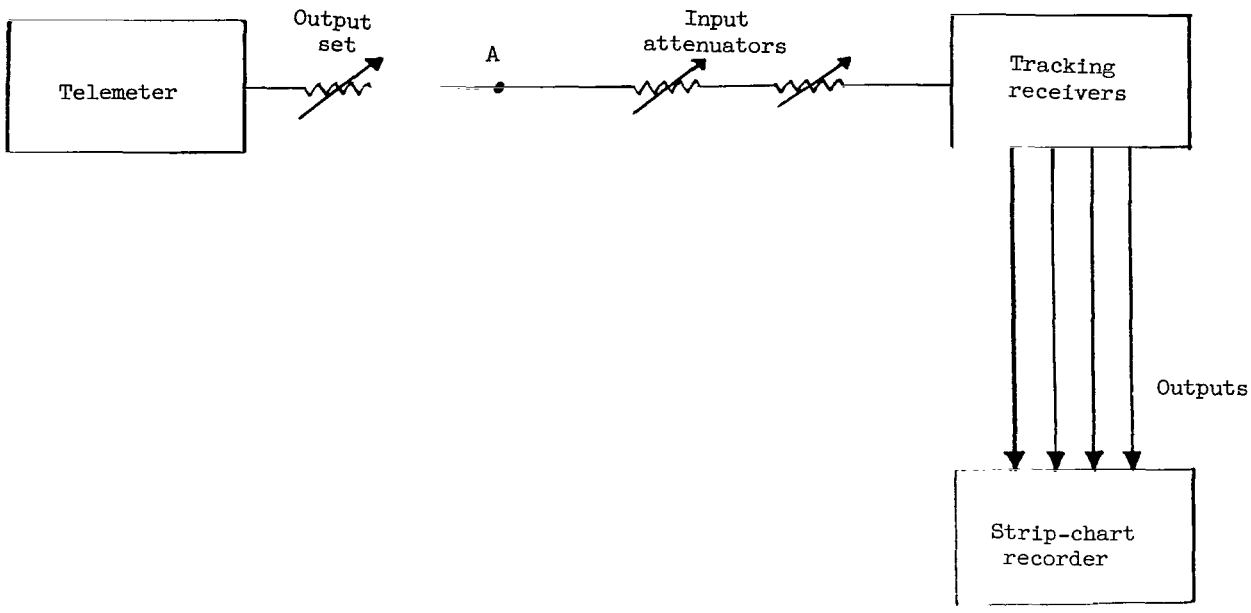

Figure IV-32.- Tracking compatibility tests.

receivers were connected together through equal line lengths so that the input signals were all of the same phase. Since the inputs differed by 0°, the outputs should be 0°. Any variance or jitter in the outputs was an error in tracking. The radio beacon showed excellent characteristics in tracking, but the telemeter signals contained modulation components which caused zero shift and jitter. Although these zero shifts and jitters were greater than desired, it was felt that satisfactory tracking could be obtained.

SECTION VI - OPERATIONAL RESULTS

After two delays caused by bad weather conditions, the final countdown for Scout ST-6 began at 12:00 midnight on August 25, 1961, and at 1:29:11 p.m. e.s.t. (18:29:11Z) of the 25th, lift-off occurred. At 18:37:56Z, Explorer XIII was injected into orbit with an unfortunate injection angle of -4.396°. This unfortunate error resulted in an abnormally low perigee of 61 nautical miles (113.5 km) which caused the orbit to decay rapidly. This departure from the nominal orbit made data acquisition extremely difficult since it was not possible to make accurate predictions of the satellite's passes. However, 21 interrogations were made during the short $2\frac{1}{2}$-day lifetime of the satellite.

Explorer XIII was successfully tracked during ascent by Wallops Island, Virginia; Blossom Point, Maryland; Locustville, Virginia; and Bermuda by using doppler techniques and by Wallops Island and Millstone Hill, Massachusetts, by using radar techniques. The radio beacon was turned on prior to lift-off and was acquired by Wallops Island and Locustville, Virginia. The exact beacon frequency was communicated to Blossom Point which was unable to pick up the radio beacon while the spacecraft was on the launch pad.

The first station to acquire Explorer XIII in orbit was Johannesburg, South Africa (JOBURG). Time of acquisition was 19:02:00Z, 24 minutes after injection. The second station was Woomera, Australia (OOMERA); acquisition time was 19:22:00Z, 44 minutes after injection.

The first readout was accomplished by East Grand Forks, Minnesota (EGRFKS). Interrogation was at 20:11:45Z), immediately after meridian crossing. Only the B telemeter was acquired at this time. The next readout was by Blossom Point, Maryland (BPOINT) at 20:17:14Z, 60 seconds after meridian crossing at BPOINT. At this time, only the A telemeter was acquired. The next contacts with the satellite were on passes 9 and 10. Only pass 9 at 26/10:02:40Z was usable and even then could only be reduced by using laborious manual techniques. The next successful passes were 13, 14, and 15, when excellent results were obtained on both telemeters. The last successful interrogations were on passes 21, 22, 23, and 28. Figure IV-33 is a world map and shows the subsatellite track for the successful interrogation passes. Table IV-3 gives a history of the interrogations.

SECTION VII - REFERENCES

IV-1. Matthews, Whitney: Earth Satellite Instrumentation. Elec. Eng., AIEE, vol. 76, no. 7, July 1957, pp. 562-567.

IV-2. Royer, G. H.: A Switching Transistor D-C to A-C Converter Having an Output Frequency Proportional to the D-C Input Voltage. Trans. American Inst. Electrical Engineers, vol. 74, pt. I, 1955, pp. 322-326.

IV-3. Baker, R. H.: Maximum Efficiency Transistor Switching Circuits. Tech. Rep. No. 110 (Contract No. AF 19(122)-458), M.I.T., Mar. 22, 1956.

IV-4. Hepler, D. S.: The Vanguard Satellite Command Receiver. NRL Rep. 5217 (Project Vanguard Rep. No. 35, Minitrack Rep. No. 6), U.S. Naval Res. Lab., Sept. 30, 1958.

IV-5. Reintjes, J. Francis, and Coate, Godfrey T.: Principles of Radar. Third ed., McGraw-Hill Book Co., Inc., 1952.

IV-6. Staff of the Lewis Research Center: Micrometeoroid Satellite (Explorer XIII) Stainless-Steel Penetration Rate Experiment. NASA TN D-1986, 1963.

THE WORLD 1:36,000,000

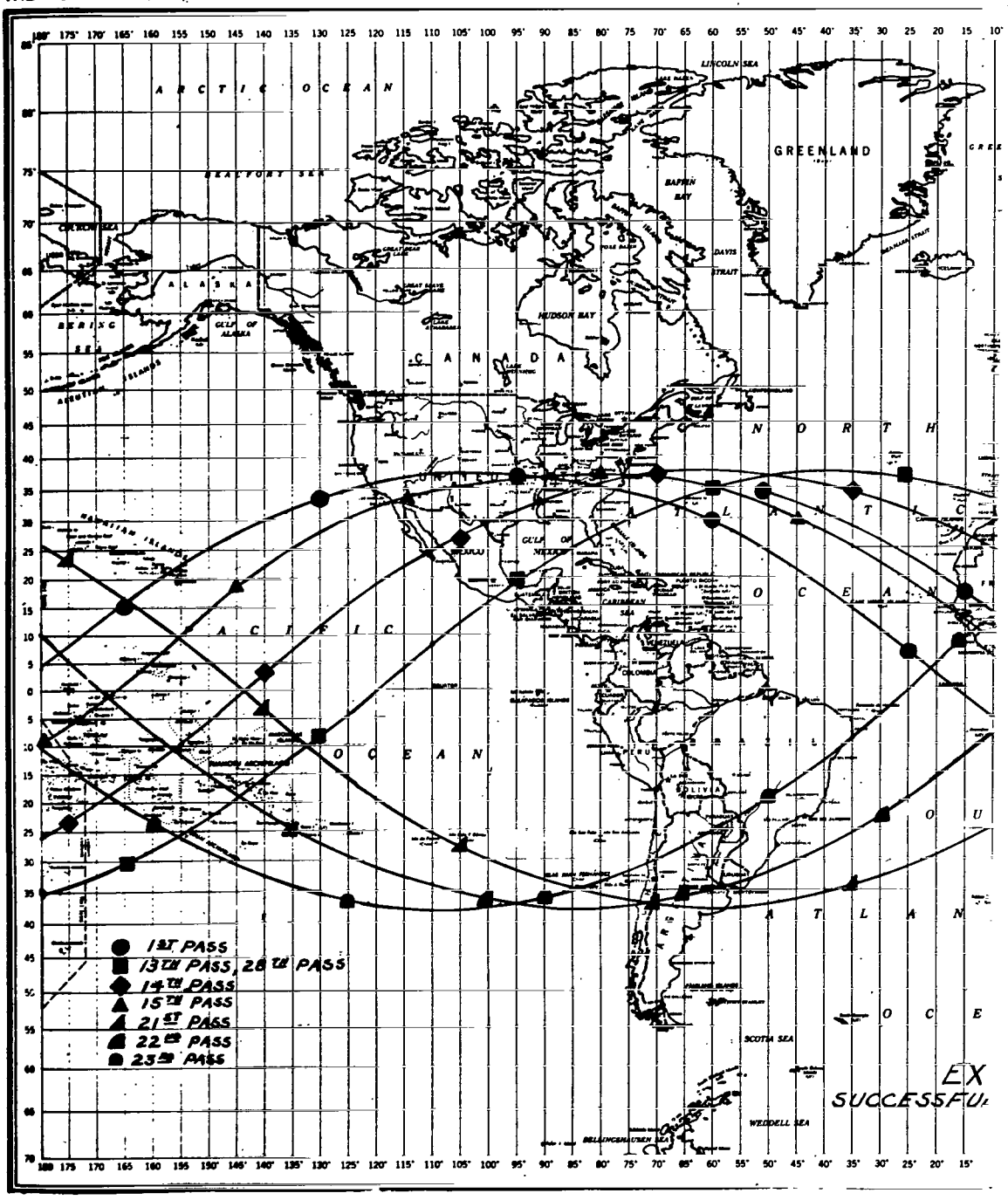

ORLD

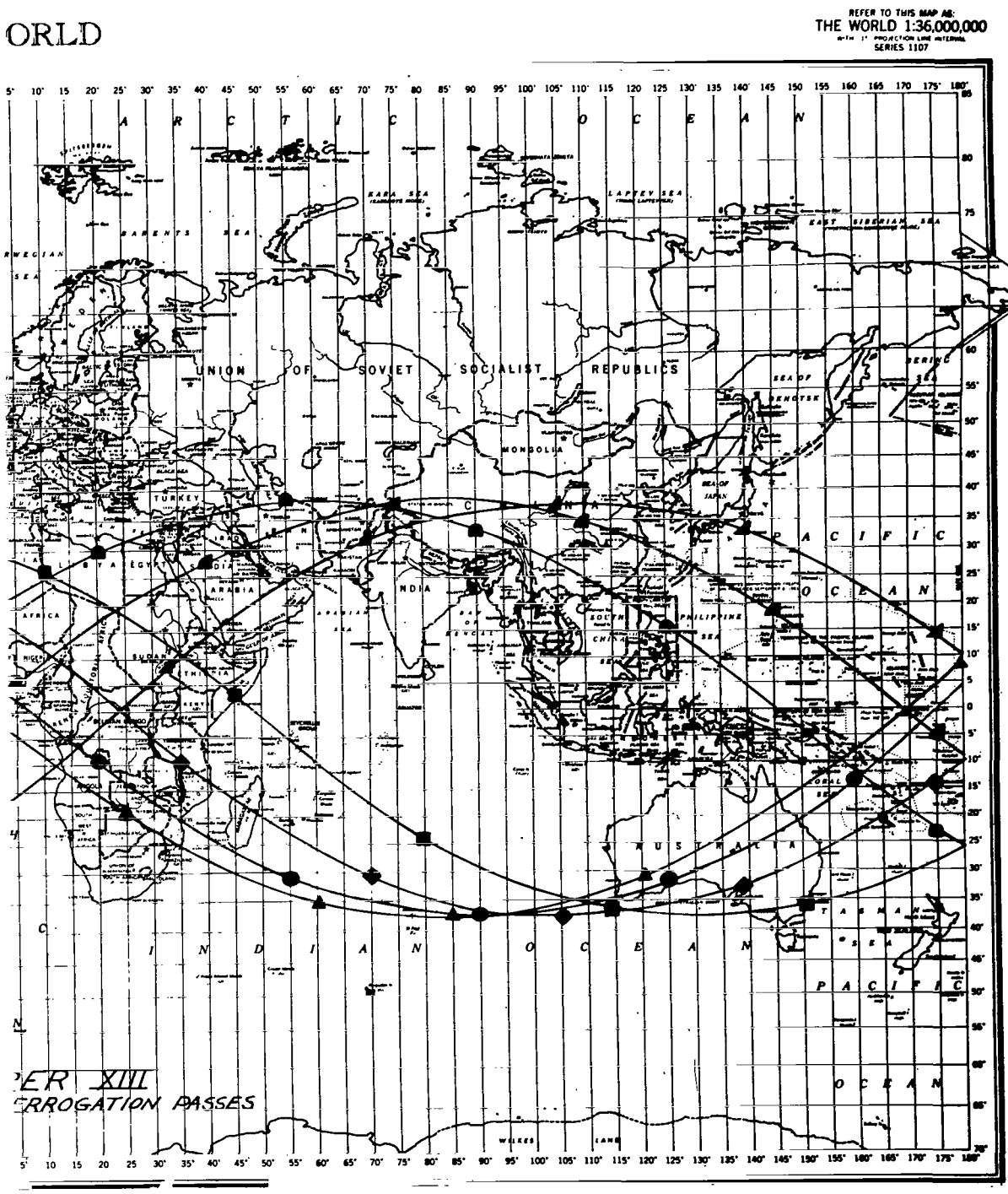

Figure IV-33.- World map of successful interrogation passes.

TABLE IV-1.- PERTINENT CHARACTERISTICS OF EXPERIMENT TELEMETERS AND RADIO BEACON

	Telemeter A	Telemeter B	Radio beacon
Type	Minitrack PDM/FM/AM; 48 channels	Same	MOPA
Emission	30A9 for 1 minute, upon interrogation only	Same	OAO
Frequency	136.200 mcps	136.860 mcps	136.860 mcps
Power output	100 mw	Same	Same
Lifetime	Indefinite	Same	1 week
Power supply	Secondary batteries (Ni-Cd) recharged by solar cells	Same	Primary batteries (Hg)
Data period	Injection to 1 year	Same	1 week

TABLE IV-2.- CHANNEL ALLOCATIONS

Channel	Telemeter A, 136.200 mcps	Telemeter B, 136.860 mcps
F_1	Zero calibrate	Zero calibrate
	Pressurized-cell-meteoroid-impact-detection system; sensitivity, 10^{-1} $\frac{gm\text{-}cm}{sec}$	Sounding-board-impact-detection system; sensitivity, 10^{-2} $\frac{gm\text{-}cm}{sec}$
F_2	Counter I; calibrate	Counter II; calibrate
F_3	Counter I; 8 count	Counter II; 8 count
F_4	Counter I; 64 count	Counter II; 64 count
F_5	Counter I; 512 count	Counter II; 512 count
F_6	Counter I; 4096 count	Counter II; 4096 count
F_7	Test solar cells; unprotected T-1	Counter III calibrate; sounding-board-impact-detection system, 10^{0} $\frac{gm\text{-}cm}{sec}$
F_8	Test solar cells; 0.006-inch glass T-2	Counter III; 8 count
F_9	Test solar cells; 0.062-inch quartz T-3	Counter III; 64 count
F_{10}	Test solar cells; unprotected T-4	Counter III; 512 count
F_{11}	Test solar cells; 0.006-inch glass T-5	Counter III; 4096 count
F_{12}	B battery voltage	A battery voltage
F_{13}	Steel-covered-grid detectors 27 to 40, 42 and 43, 0.003 inch	Steel-covered-grid detectors 1 to 8; 0.003 inch
F_{14}	Steel-covered-grid detectors 44 to 55 and 57 to 60, 0.003 inch	Steel-covered-grid detectors 9 to 11 and 13 to 17, 0.003 inch
F_{15}	Steel-covered-grid detectors 12, 26, 41, and 56, 0.006 inch	Steel-covered-grid detectors 18 to 25, 0.006 inch
F_{16}	A battery voltage	B battery voltage
D_1	Frame sync	Frame sync
S_1	Identification, zero ohms	Identification, 470 ohms
D_2	Calibrate, full scale	Calibrate, full scale
S_2	Calibrate, zero	Calibrate, zero
D_3	Calibrate, zero	Calibrate, zero
S_3	Calibrate, full scale	Calibrate, full scale
D_4	Temperature electronics package (35A2)	Temperature electronics package (35A2)
S_4	Pressurized-cell detectors 36 to 40 and 116 to 120, 0.0025 inch	Pressurized-cell detectors 76 to 80 and 156 to 160, 0.0025 inch
D_5	Pressurized-cell detectors 1 to 5 and 81 to 85, 0.001 inch	Pressurized-cell detectors 41 to 45 and 121 to 125, 0.001 inch
S_5	Pressurized-cell detectors 31 to 35 and 111 to 115, 0.001 inch	Pressurized-cell detectors, 71 to 75 and 151 to 155, 0.001 inch

TABLE IV-2.- CHANNEL ALLOCATIONS - Concluded

Channel	Telemeter A, 136.200 mcps	Telemeter B, 136.860 mcps
D_6	Pressurized-cell detectors 6 to 10 and 86 to 90, 0.005 inch	Pressurized-cell detectors 46 to 50 and 126 to 130, 0.005 inch
S_6	Pressurized-cell detectors 26 to 30 and 106 to 110, 0.0015 inch	Pressurized-cell detectors 66 to 70 and 146 to 150, 0.0015 inch
D_7	Pressurized-cell detectors 11 to 15 and 91 to 95, 0.0015 inch	Pressurized-cell detectors 51 to 55 and 131 to 135, 0.0015 inch
S_7	Pressurized-cell detectors 21 to 25 and 101 to 105, 0.002 inch	Pressurized-cell detectors 61 to 65 and 141 to 145, 0.002 inch
D_8	Pressurized-cell detectors 16 to 20 and 96 to 100, 0.001 inch	Pressurized-cell detectors 56 to 60 and 136 to 140, 0.001 inch
S_8	Forward-shell temperature (Low range, GB25J1)	Forward-shell temperature (Low range, GB25J1)
D_9	Forward-shell temperature (High range, GA42J3)	Forward-shell temperature (High range, GA42J3)
S_9	Test solar cells, T1 and T2 Temperature (35A2)	Test solar cell T3 Temperature (35A2)
D_{10}	Pressurized-cell detectors Temperature (Low range, GB25J1)	Pressurized-cell detectors Temperature (Low range, GB25J1)
S_{10}	Pressurized-cell detectors Temperature (High range, GA42J3)	Pressurized-cell detectors Temperature (High range, GA42J3)
D_{11}	Power-supply solar cell B4 Temperature (35A2)	Power-supply solar cell B2 Temperature (35A2)
S_{11}	Steel-covered-grid detector Temperature (38C2)	Steel-covered-grid detector Temperature (38C2)
D_{12}	Steel-covered-grid detector Temperature (38C2)	Steel-covered-grid detector Temperature (38C2)
S_{12}	Guard	Guard
D_{13}	Cd S Cell	Cd S Cell
S_{13}	Cd S Cell temperature (35A2)	Cd S Cell temperature (35A2)
D_{14}	Copper-wire-card detectors 1 to 8, 0.003 inch	Copper-wire-card detectors 17 to 24, 0.003 inch
S_{14}	Copper-wire-card detectors 9 to 16, 0.003 inch	Copper-wire-card detectors 25 to 32, 0.003 inch
D_{15}	Copper-wire-card detectors 33 to 35, 0.002 inch	Copper-wire-card detectors 40 to 43, 0.002 inch
S_{15}	Copper-wire-card detectors 36 to 39, 0.002 inch	Copper-wire-card detectors 44 to 46, 0.002 inch
D_{16}	Copper-wire-card detectors Temperature (35A2)	Copper-wire-card detectors Temperature (35A2)
S_{16}	Telemeter pressurization	Telemeter pressurization

TABLE IV-3.- INTERROGATION HISTORY

Orbit	Date/time	Minitrack station	Tape	Telemeter	Data-reduction process
Launch	25/18:29:44	Blossom Point	122A001	None	None
1	25/20:11:45	Grand Forks	122N001	B	Automatic
1	25/20:11:45	Blossom Point	122A002	B	Automatic
1	25/20:17:14	Blossom Point	122A002	A	Manual*
2	25/21:59:40	Fort Myers	122D001	None	None
7	26/06:34:00	Santiago	122J001	None	None
8	26/08:32:15	Santiago	122J001	None	None
9	26/10:02:40	Antofagasta	122H001	A	Manual
9	26/10:02:40	Antofagasta	122H001	B	Manual
10	26/11:46:00	Quito	122F001	A	Manual
10	26/11:55:00	Quito	122F001	B	Manual
13	26/15:13:30	Fort Myers	122D001	A	Automatic
13	26/15:15:02	Fort Myers	122D001	B	Automatic
13	26/15:13:30	Blossom Point	122A003	A	Automatic
13	26/15:15:02	Blossom Point	122A003	B	Automatic
14	26/16:58:06	Blossom Point	122A004	A	Automatic
14	26/16:58:06	Blossom Point	122A004	B	Automatic
14	26/16:58:06	Fort Myers	122D002	A	Automatic
14	26/16:58:06	Fort Myers	122D002	B	Automatic
15	26/18:40:57	Fort Myers	122D002	A	Automatic
15	26/18:40:57	Fort Myers	122D002	B	Automatic
20	27/03:03:00	Santiago	122J002	A	Manual
20	27/03:03:00	Santiago	122J002	B	None
21	27/04:45:56	Santiago	122J003	A	Automatic
21	27/04:45:56	Santiago	122J003	B	Automatic
22	27/06:21:30	Santiago	122J003	A	Automatic
22	27/06:21:30	Santiago	122J003	B	Automatic
23	27/08:03:14	Antofagasta	122H001	A	Automatic
23	27/08:03:14	Antofagasta	122H001	B	Automatic
25	27/11:15:40	Lima	122G01	None	None
27	27/14:03:00	Woomera	122-1	None	None
28	27/15:42:15	Woomera	122-1	A	Automatic
28	27/15:42:15	Woomera	122-1	B	Automatic
35	28/02:00:03	Antofagasta	122H001	A	Manual**
35	28/02:00:03	Antofagasta	122H001	B	Manual**
40	28/08:46:00	Antofagasta	122H001	B	Manual**

*Special process by GSFC.

**The temperatures of all systems had increased beyond design limits as a result of aerodynamic heating so that these data could not be used.

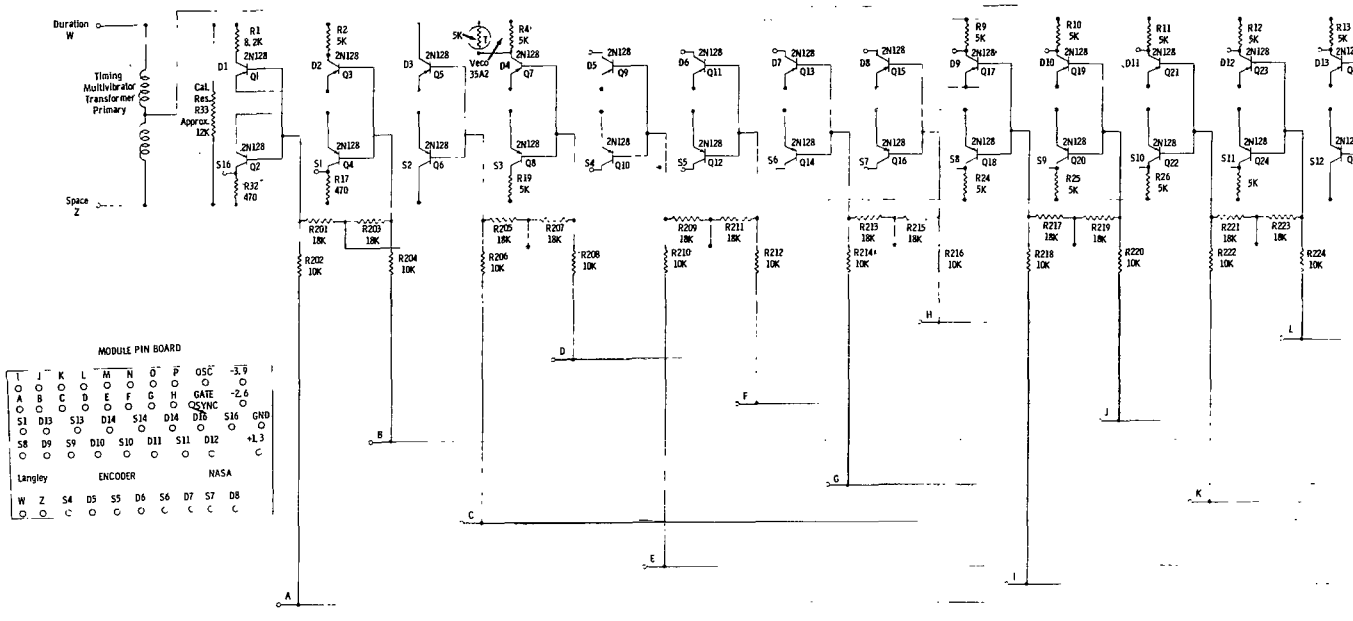
Duration W
Timing Multivibrator Transformer Primary
Space Z
Cal. Res. R33 Approx 12K
MODULE PIN BOARD
Langley
ENCODER
NASA
Vero 35A2
5K
2N128
R1 8.2K
R2 5K
R4 5K
R9 5K
R10 5K
R11 5K
R12 5K
R13 5K
R17 470
R19 5K
R24 5K
R25 5K
R26 5K
R32 470
R201 18K
R202 10K
R203 18K
R204 10K
R205 18K
R206 10K
R207 18K
R208 10K
R209 18K
R210 10K
R211 18K
R212 10K
R213 18K
R214 10K
R215 18K
R216 10K
R217 18K
R218 10K
R219 18K
R220 10K
R221 18K
R222 10K
R223 18K
R224 10K

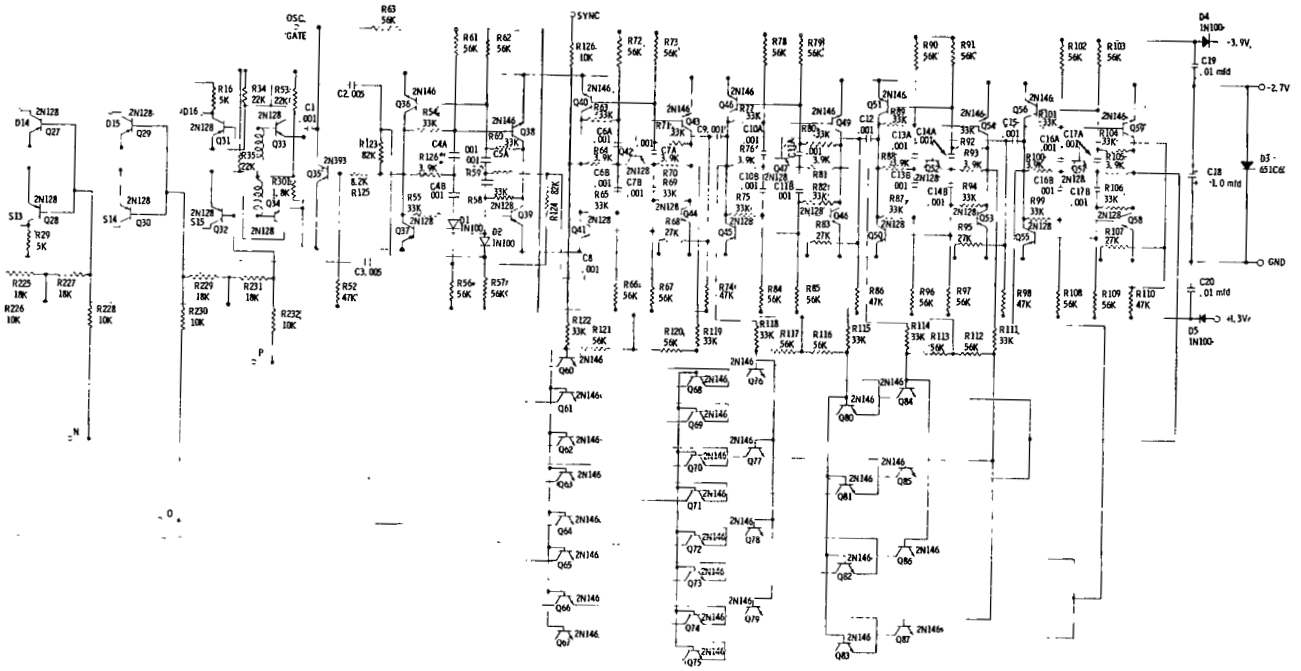

Circuit diagram 1.- Forty-eight channel encoder module schematic.

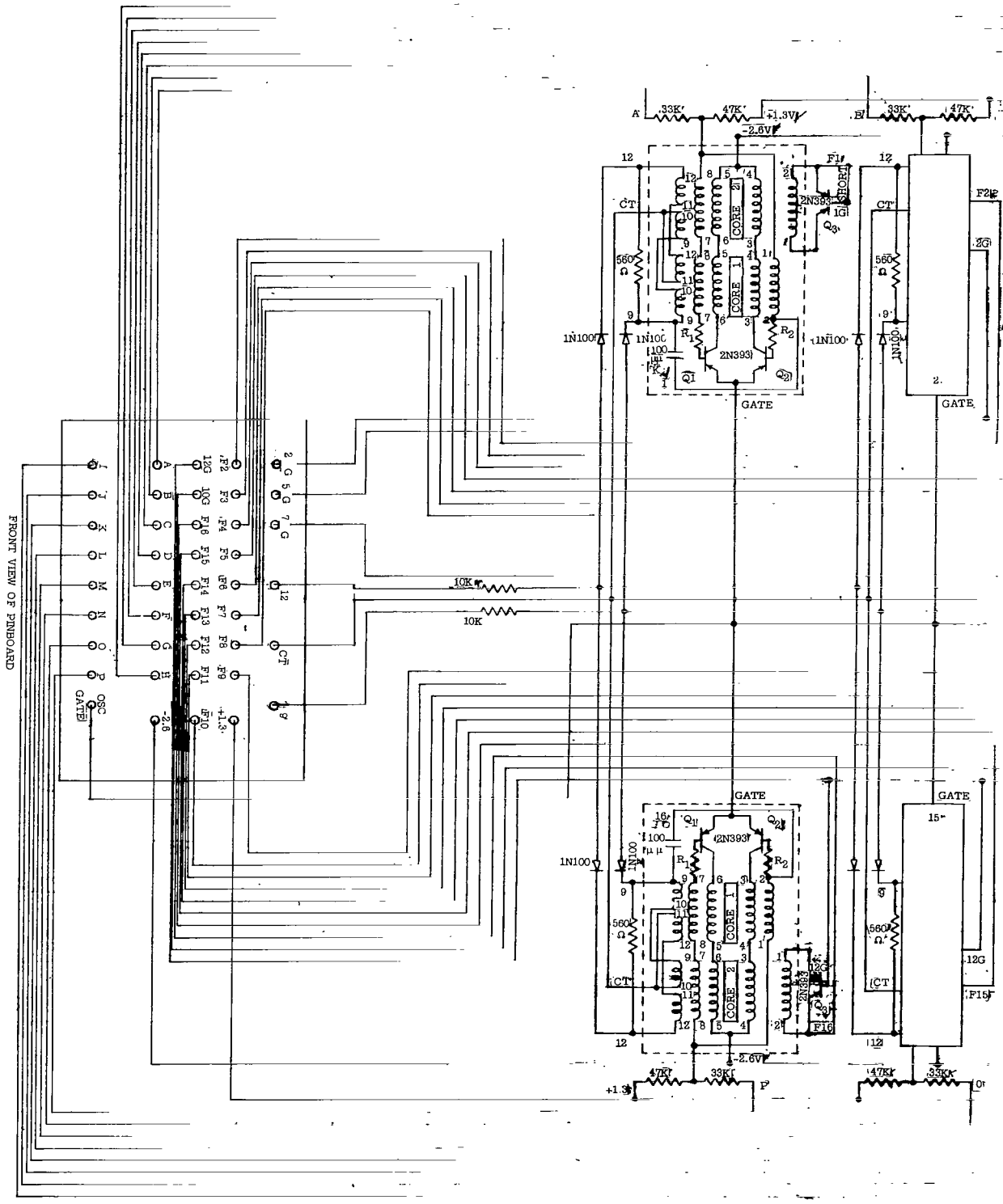
FRONT VIEW OF PINBOARD
GATE
2N393
1N100
560 Ω
10K
33K
47K
+1.3V
-2.6V
CORE
SHORT

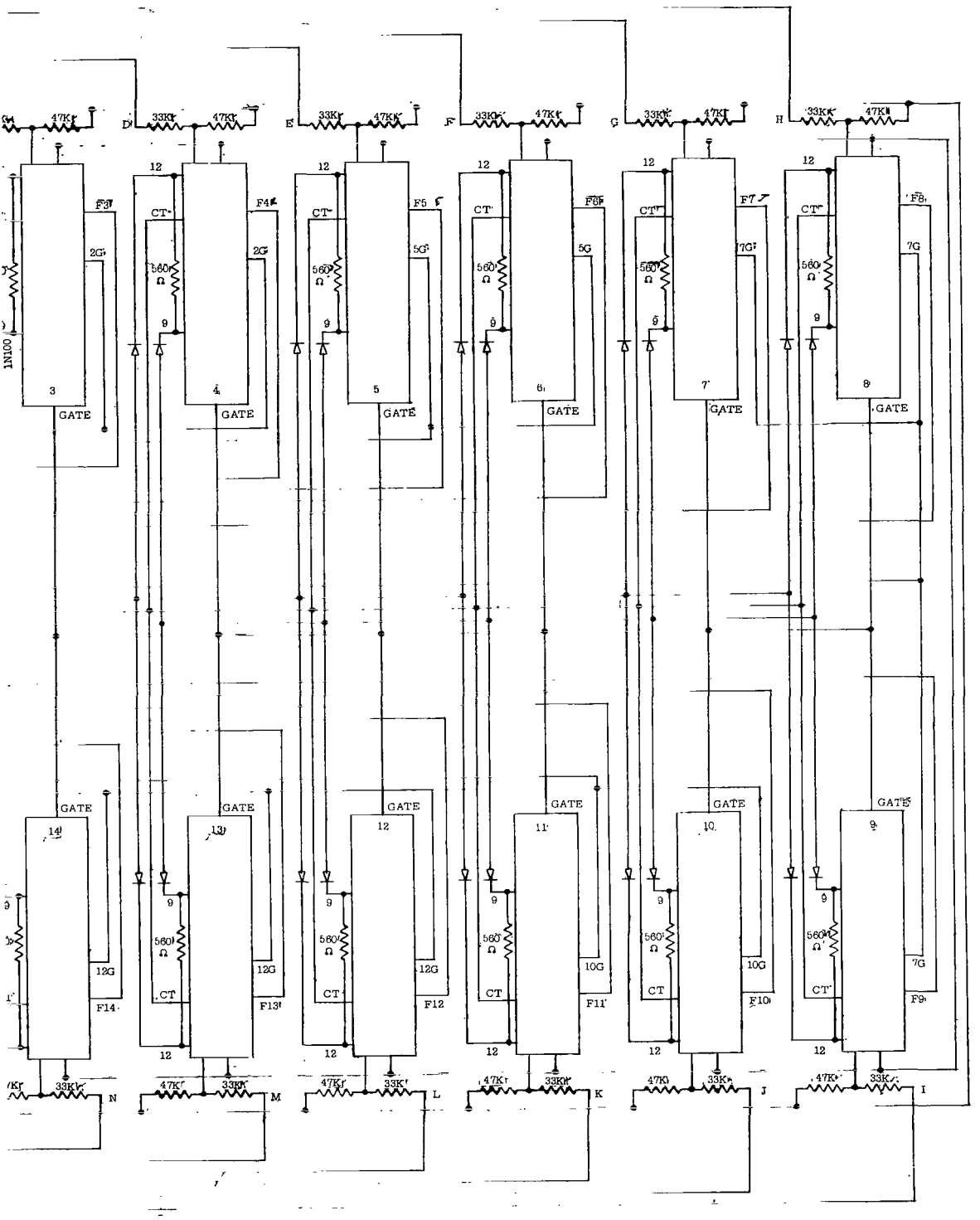

Circuit diagram 2.- Subcarrier oscillator module.

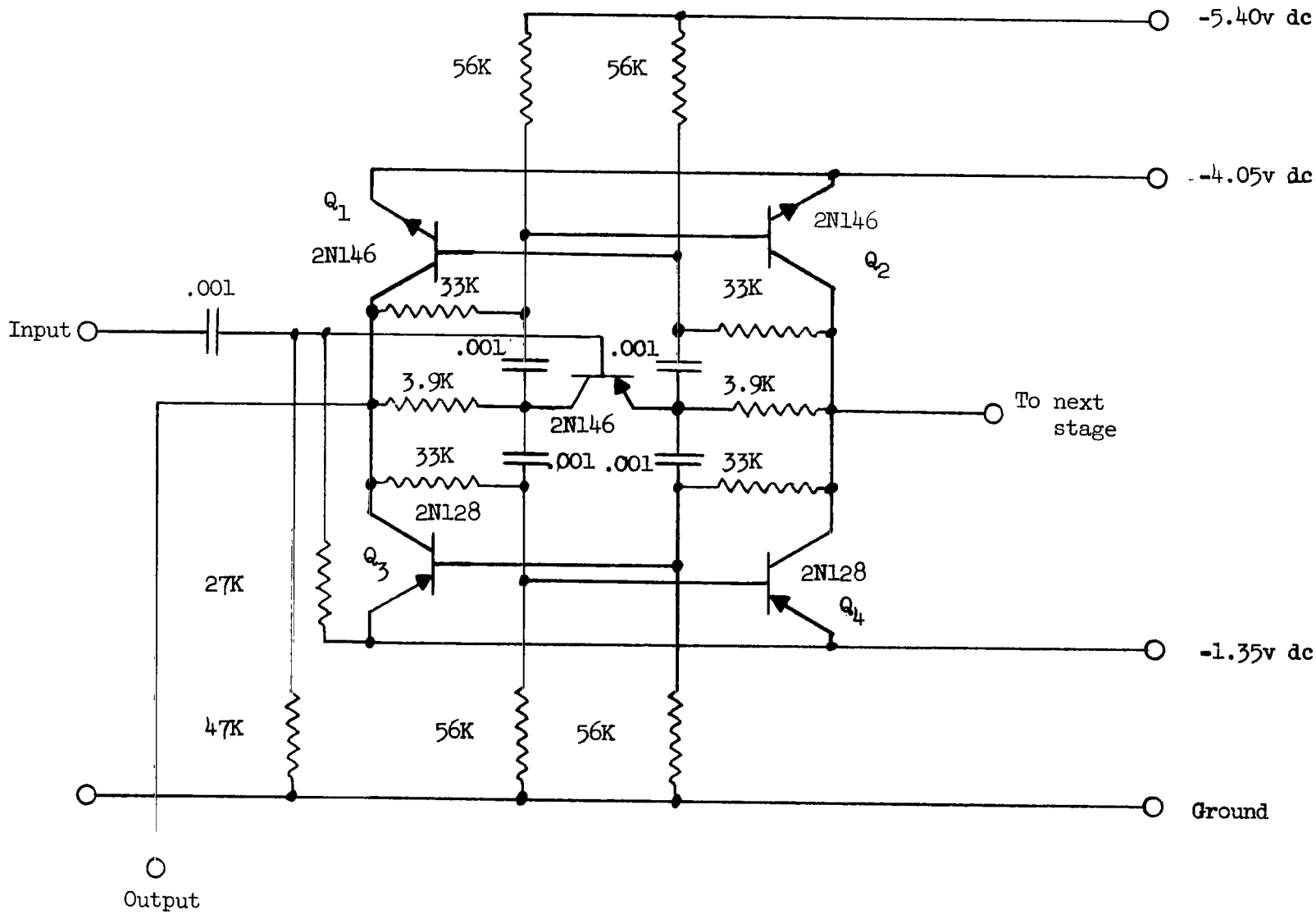

Circuit diagram 3.- Five-transistor complementary flip-flop circuit.

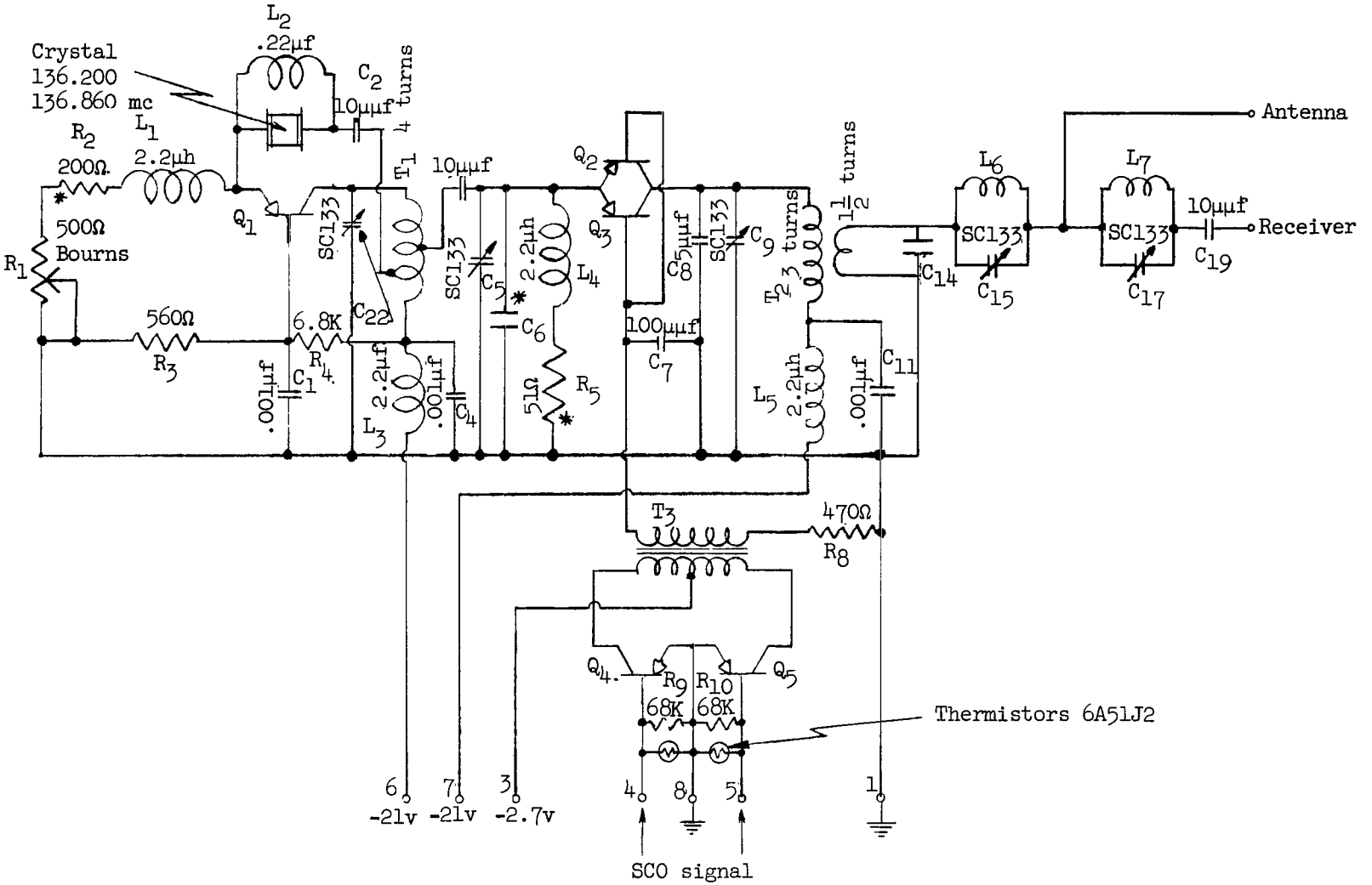

Q_1, Q_2, Q_3	2N1195
Q_4, Q_5	2N1303

Circuit diagram 4.- Transmitter module schematic.

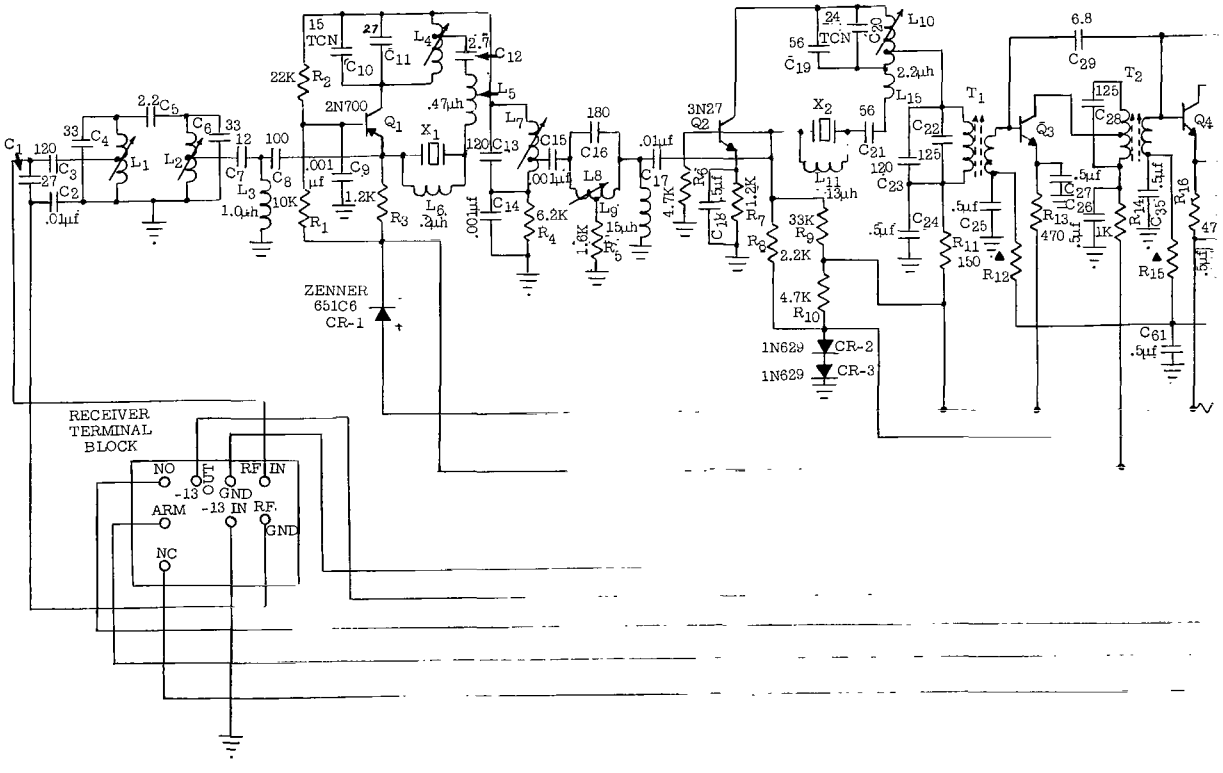
RECEIVER
TERMINAL
BLOCK
NO
-13
GND
RF IN
ARM
-13 IN
RF.
GND
NC
ZENNER
651C6
CR-1
1N629
CR-2
1N629
CR-3
2N700
Q1
3N27
Q2
Q3
Q4
T1
T2
X1
X2
L1
L2
L3
L4
L5
L6
L7
L8
L9
L10
L11
L15
C1
C2
C3
C4
C5
C6
C7
C8
C9
C10
C11
C12
C13
C14
C15
C16
C17
C18
C19
C21
C22
C23
C24
C25
C26
C27
C28
C29
C33
C61
R1
R2
R3
R4
R5
R6
R7
R8
R9
R10
R11
R12
R13
R14
R15
R16

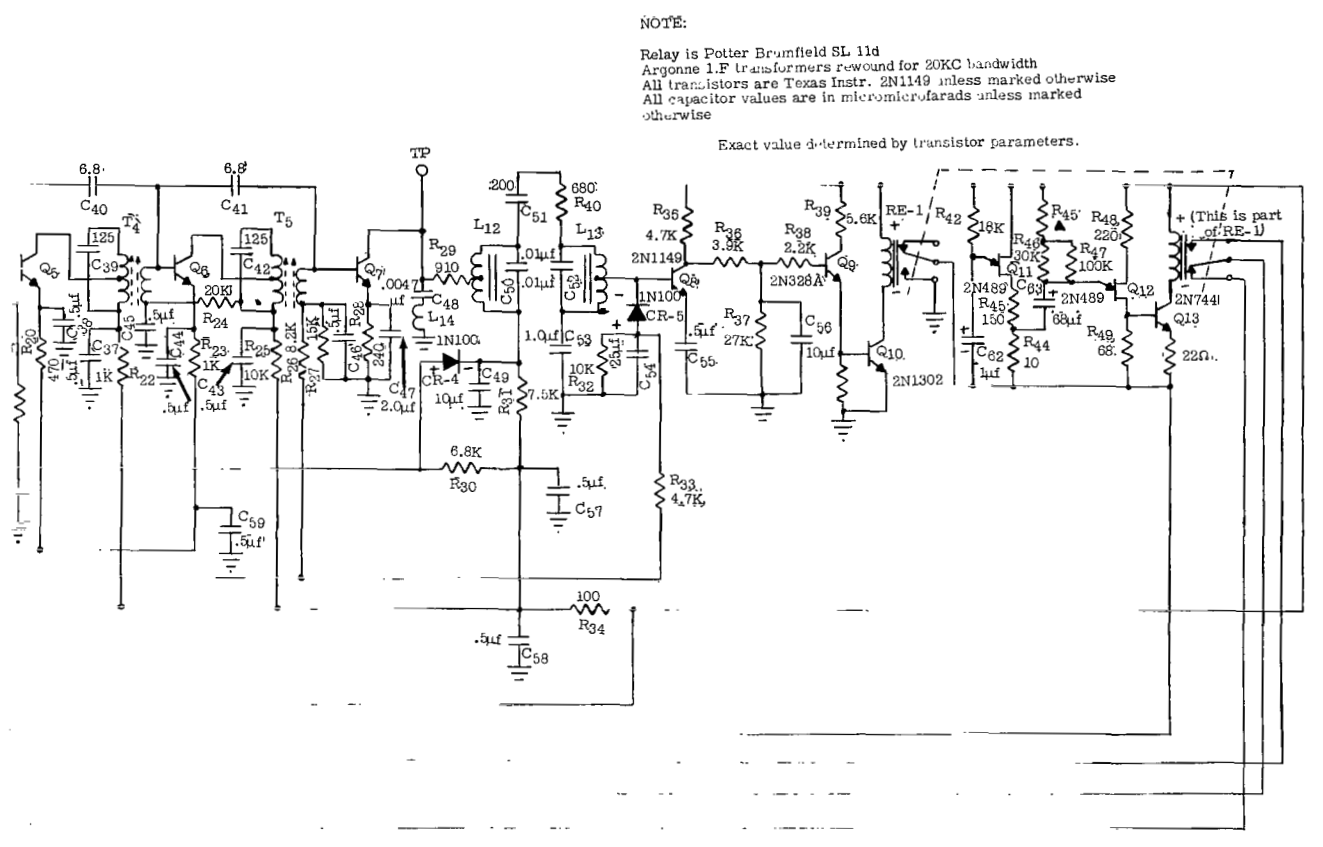

Circuit diagram 5.- Schematic of command receiver.

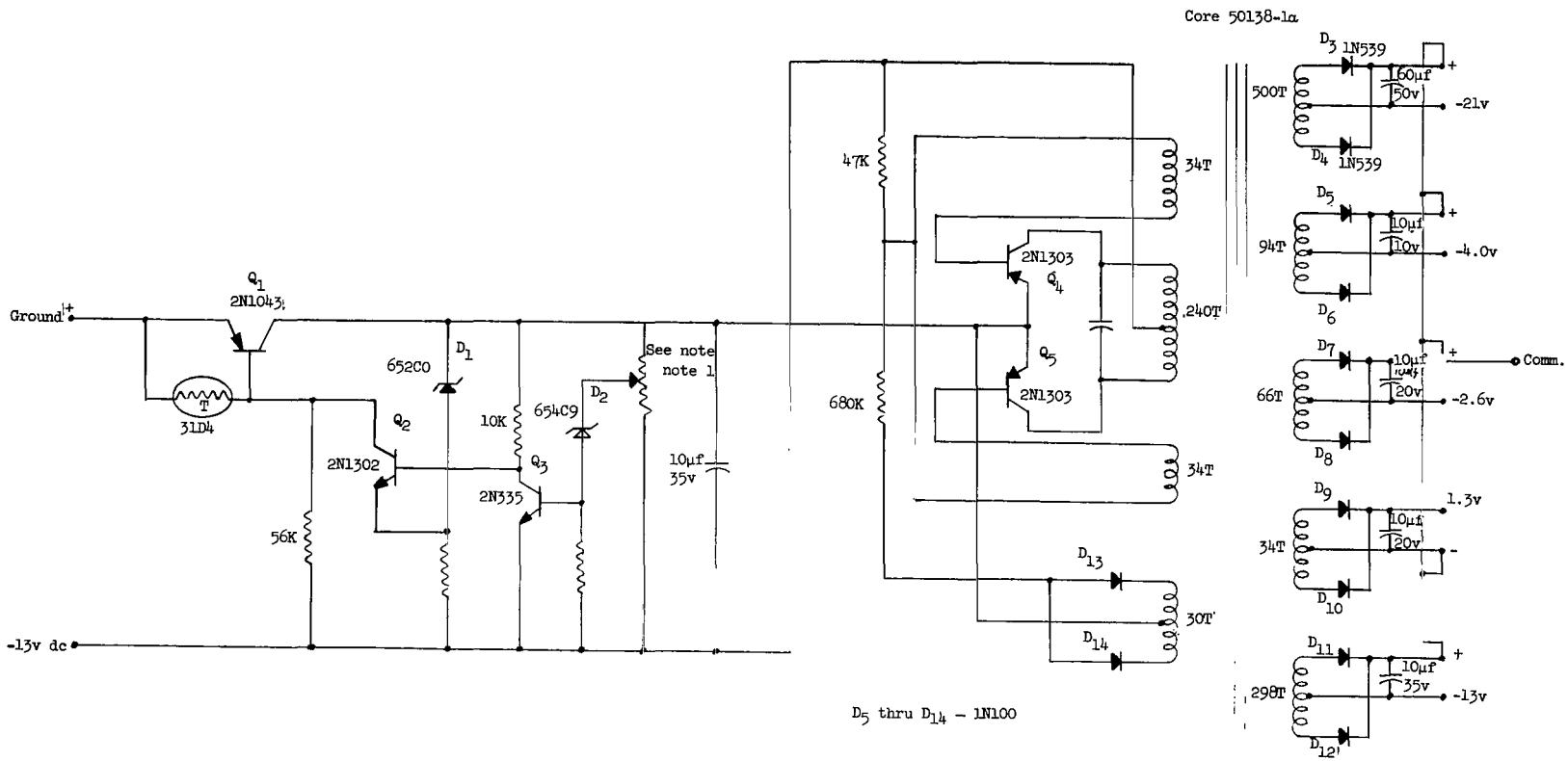

Circuit diagram 6.- Dc-dc converter schematic.